NKS-493
ISBN 978-87-7893-590-8

CFD and system code modelling of passive safety system performance

Ari Silde[1]

Afeef Murad[1]

Marton Szogradi[1]

[1] VTT Technical Research Centre of Finland Ltd.

January 2025

Abstract

Apros system code model and the OPenFOAM CFD model were created and the preliminary simulations were conducted for the planned arrangement of the Panda facility PCCS experiment P1A4. The Apros model consisted of the whole system including the containment vessel, the PCC pipe, the PCCS water circulation loop and the water pool. The OpenFOAM model included only the containment vessel, the PCC pipe and the steam injection lines inside the vessel.

Quasi-steady conditions of the whole test apparatus were calculated with Apros varying the steam injection rate. The vessel pressure, gas temperatures, steam mole fractions, water mass flow rate in the PCCS circulation loop and water inlet temperature of the PCC pipe were given as boundary conditions for the CFD simulation. The purpose of the work was to learn and prepare the Apros and CFD model capabilities for future simulation of the Panda test P1A4 to be conducted in the OECD/NEA benchmark exercise.

The Apros results showed that the system model works as expected and the results are qualitatively reasonable. Steam injection rate of 0.01 kg/s seemed to produce quasi-steady conditions during 55 hours simulation.

The CFD simulation exceeded 1720 s until finalisation of this report. The preliminary CFD simulation results were promising.

Some model improvements should be done for the future work. More suitable heat transfer correlation for a single-pipe PCCS should be implemented in Apros. Also a multi-node pool model should be developed.

What comes to the CFD model, an investigation regarding the numerical schemes is recommended. Furthermore, a denser mesh should be developed by refining the regions close to the PCCS pipe and the vessel walls where condensation occurs.

Key words

SMR, BWRX-300, passive safety system, modelling, Apros, OpenFOAM

NKS-493
ISBN 978-87-7893-590-8
Electronic report, January 2025

NKS Secretariat
P.O. Box 49
DK - 4000 Roskilde, Denmark
Phone +45 4677 4041
www.nks.org
e-mail nks@nks.org

CFD and system code modelling of passive safety system performance

Final Report from the NKS-R PAS-SMR activity

(Contract: AFT/NKS-R(24)141/7)

Ari Silde[1]
Afeef Murad[1]
Marton Szogradi[1],

[1]Technical Research Centre of Finland VTT

Table of contents

1. Introduction

Small modular rector (SMR) technology is a very likely candidate for new nuclear power plants in Europe including Nordic countries. Several designs of SMRs are currently under development or ready to be deployed. Passive safety systems are widely used in all SMR designs and they are the key factor for enhanced safety of SMRs.

In this work, performance and modelling capabilities of passive safety systems of SMRs will be studied using the system code Apros and OpenFOAM CFD software.

The work is started with a literatue review where special features of BWRX-300-relevant passive cooling systems are mapped to understand the main critical functions and phenomena of the systems (section 3). After that a representative experiment is selected to be modelled with the CFD and system code methods. The selected experiment is a coming large-scale PANDA experiment P1A4 where a Passive Containment Cooling System (PCCS) performance will be studies (section 4.1). The test arrangement consists of a vertical single-pipe heat exchanger (HEX) including a liquid water circulation loop and a water pool. The HEX pipe (called here also as PCC pipe) is located vertically inside the PANDA vessel atmosphere which represents the containment volume. Relevant simulation models are built with the Apros and CFD OpenFOAM softwares (sections 4.2 and 4.3). Finally, a principal functionality of the models are checked and a preliminary simulations and benchmarks between OpenFOAM and Apros are conducted (sections 4.2.2 and 4.3.2). Because there is still no experimental data (the experiment P1A4 will be conducted in spring 2025), no comparison with the measurements cannot be made at this stage.

2. Objectives

The main aim of the work is to develop expertise in advanced modelling capabilities for passive safety systems, particularly related to the GE BWRX-300 design. The work focuses at this stage on the performance of PCCS. Both system code and CFD methods are applied parallel. It is planned that the simulation results will be later compared with the experimental data in blind and open benchmark exercises.

The work has also an educational aspect. A new specialist is familiarised and trained with the CFD modelling starting with a model simple enough and continue step-by-step to more detailed modelling approach. Also from this point of view, a single-pipe PCCS test P1A4 at the PANDA facility is very suitable and simple test arrangement for the learning purposes. Also participation in the coming benchmark exercise would give a great chance to meet other simulation experts and create a network that is important to facilitate licensing process of SMRs in Nordic countries and develop expertise in analyses of passive safety system performance.

3. General description of special features of BWRX-300-relevant passive cooling systems

This section provides a basis for the subsequent computer-aided analyses, laying out the key parameters and approximations considering the mentioned unit's safety systems, more precisely the Isolation Condenser System (ICS) and Passive Containment Cooling System (PCCS). Section 3.1.1 provides information concerning the BWRX-300 ICS while Section 3.1.2 disseminates publicly available information on the PCCS.

In addition, several prominent experimental facilities and corresponding activities will be discussed to elicit a frame of reference in terms of thermal-hydraulic phenomena and modelling challenges. The Sections 3.2.1 and 3.2.2 describe the PERSEO facility of SIET (Mascari et al. 2023; Narcisi et al., 2021) and the PASCAL facility at Korea Atomic Energy Research Institute (KAERI) (Jeon et al., 2013; Jeon et al., 2015; Lee et al., 2024) to bring forth submerged heat exchanger examples, i.e. ICS analogues. As for PCCS-relevant test rigs the PANDA facility of Paul Scherrer Institut (PSI) (Kapulla et al., 2022; Paladino et al., 2022; Paranjape et al., 2024) will be discussed in Section 3.2.3.

These three facilities are discussed in the present report in the context of specific tests, e.g. the observed phenomena in the PANDA vessel with respect to the H2P6 tests focusing on stratification and condensation in the presence of a non-condensable agent. Most of the examples will entail validation and verification activities mainly tied to lumped parameter codes, to a smaller extent revolving around CFD analysis. Nonetheless, the phenomenology of the investigated aspects is very much relevant for subsequent CFD studies performed by VTT within the NKS project.

3.1 Features of the BWRX-300 unit

The fundamentals of the boiling water reactor (BWR) technology were laid down by Argonne National Laboratory and General Electric (GE), starting from the 1950s. The evolution of the concept traversed over two separate lineages; one based on forced circulation (more populous branch) and another relying on natural circulation. The two tracks merged under the umbrella of the Simplified Boiling Water Reactor (SBWR) in the 1980s and early 1990s. Afterwards GE scaled up the SBWR to obtain a more economically viable product, the end-result of these activities was the Economic Simplified Boiling Water Reactor (ESBWR). The hereby discussed BWRX-300 unit is the successor of the ESBWR, with a smaller core and dry containment. The reactor pressure vessel (RPV) retained its aspect ratio from the ESBWR meaning that the tall, lean vessel enhances natural circulation without necessary modifications in core height. This also implies that BWRX-300 is compatible with fuel bundle designs in use nowadays, at least in terms of geometry (Hitachi, 2023). Compared to ESBWR, the main simplifications are:

- The implementation of integral RPV dual quarter-turn isolation valves to mitigate the impacts of Loss-Of-Coolant Accidents (LOCAs), the strategy eliminates non-isolable breaks greater than 19 mm of nominal size.
- The ICS also acts as Emergency Core Cooling System (ECCS) utilizing natural circulation without an external power source.
- Safety Relief Valves (SRVs) were eliminated from the design, their function is fulfilled by the ICS[1].

[1] The justification here is that statistically SRVs have been the most likely cause of a LOCA in BWRs.

- GE claims that the unit was designed to be able to accommodate more commercial off-the-shelf equipment compared to previous BWRs (e.g. turbogenerators).

General attributes of the ESBWR and BWRX-300 designs are provided in Table 1 below. The schematics of major systems and the cross-section of the reactor building are depicted in Figure 1 and Figure 2, respectively.

Table 1. ESBWR vs. BWRX-300 (Hitachi, 2023).

Attribute	**ESBWR**	**BWRX-300**
Gross electrical power [MWe]	~1600	~300
Thermal power [MWth]	4500	870
Coolant circulation	natural circulation	natural circulation
Primary system nominal pressure [bar]	72 (abs.)	72 (abs.)
RPV inner diameter - D_i [m]	7.1	4.0
RPV wall thickness [mm]	n.a.	136 (w cladding)
RPV height - H [m]	27.6	26.0
Active core height [m]	n.a.	3.8
Fuel type	GNF2e	GNF2
No. of fuel assemblies [-]	1132	240
Control rod type	Cruciform B_4C or Hf	Cruciform B_4C or Hf
Control rod drive	Fine Motion Control Rod Drive (FMCRD)	Fine Motion Control Rod Drive (FMCRD)
No. of control rods [-]	269	57
Primary containment vessel type	Reinforced concrete	Steel-plate composite
Primary containment vessel cooling system	Passive	Passive
Isolation makeup	Isolation condensers (passive)	Isolation condensers (passive)
ECCS	Passive	Passive
Shutdown cooling	Non-safety related	Safety Category 3 (SC3) [2]
Emergency AC power	Non-safety related	Two SC3 diesel generators

[2] SC3 is the classification of structures, systems and components (SSCs) that are needed only after the first seven days of the given event.

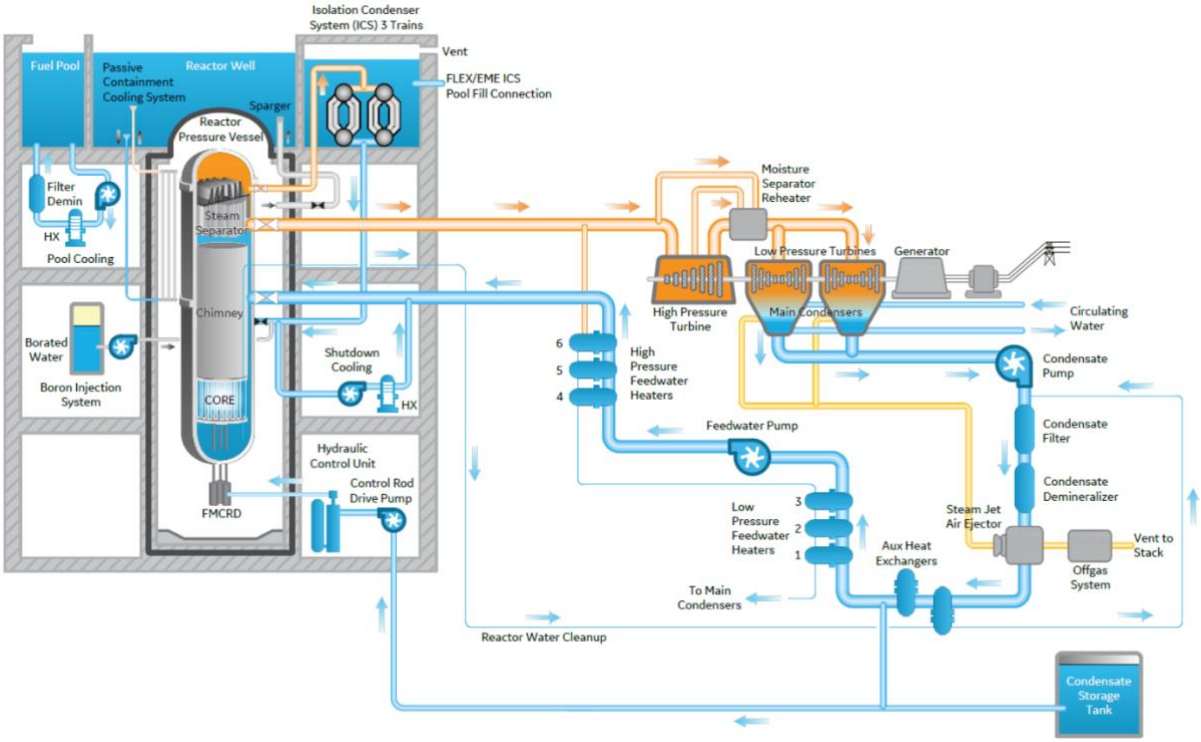

Figure 1. BWRX-300 primary and secondary systems' layout (Hitachi, 2023).

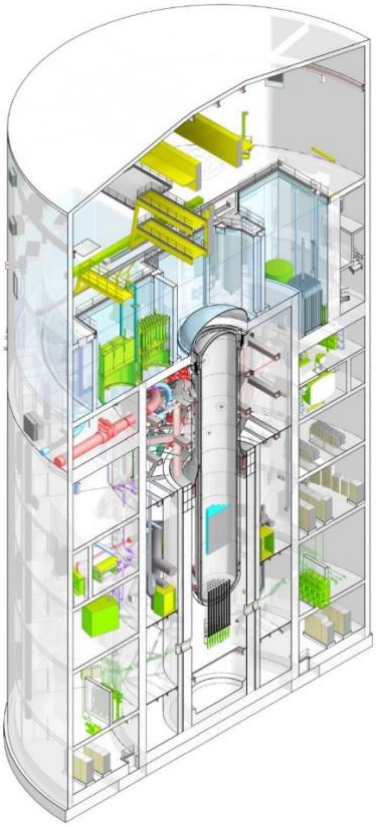

Figure 2. BWRX-300 nuclear island cross-section (Hitachi, 2023).

3.1.1 Isolation Condenser System (ICS)

The Isolation Condenser System (ICS) connects the RPV to the dedicated cooling pools (ultimate heat sinks) which are located above the RPV at the same elevation as the top of the reactor well. The system comprises three independent trains, each featuring a condensate return line, a steam line, a pair of Heat EXchangers (HEXs) and a pool (Figure 3, ICS (A, B, C)). The pools remain in a stand-by state during normal operation, maintaining a 1 bar absolute cover gas (air) pressure with vent lines to the atmosphere. Each train has a capacity of ~33 MW which corresponds to ~3.8 % of the rated thermal power (The official GE description notes 3.7 % (Hitachi, 2023)). The operational principle of the ICS resembles the usual arrangement, promoting a buoyancy-driven flow between the heat source (RPV) and heat sink (pools). Should the main condenser become offline and the RPV isolated, the ICS condensate return line valves open allowing the condensate to enter the RPV in the chimney region below the feedwater nozzles. The generated steam thereafter exits the RPV via the steam lines, finally condensing in the tube bundles of the HEXs.

According to the specifications, only one ICS train is required to handle Anticipated Operational Occurrences (AOOs) while two trains are required in case of a LOCA[3] (Hitachi, 2023), assuming the failure of a train. Ref. (Hitachi, 2023) also claims that with two trains the decay heat removal function can be fulfilled for seven consecutive days without operator action, afterwards the pool inventory is supposed to be replenished via the external pool connections (see Figure 1). Main geometry specifications and schematics are provided in Table 2 and Figure 4, respectively. It has to be emphasized that ref. (Pomogaev et al., 2022) did not disclose the source of the geometry specifications thus they can only be regarded as coarse approximations. Also note that the collector length is defined as 6000 mm in Table 2 while Figure 4 denotes 7000 mm indicating large uncertainties in public documents.

Table 2. Geometry specifications of the ICS HEX based on ref. (Pomogaev et al., 2022).

Attribute	
Maximum design heat capacity [MWth]	~33
No. of heat exchanger tubes per HEX pair	360
D_i of collector [mm]	630
Top/bottom collector length [mm]	6000
Length of HEX pipes [mm]	1800
D_i of HEX tubes [mm]	20
Wall thickness of HEX tubes [mm]	3
Material	SS316

[3] No specifics were provided concerning the LOCA scenario in the noted reference.

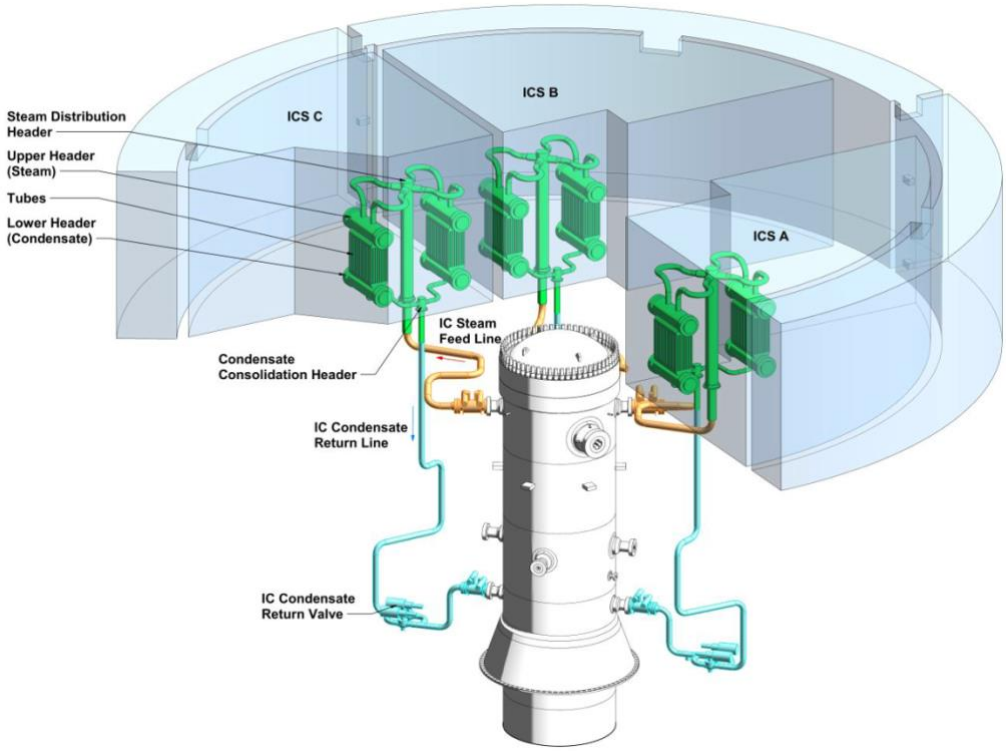

Figure 3. ICSs in the reactor building (Hitachi, 2023).

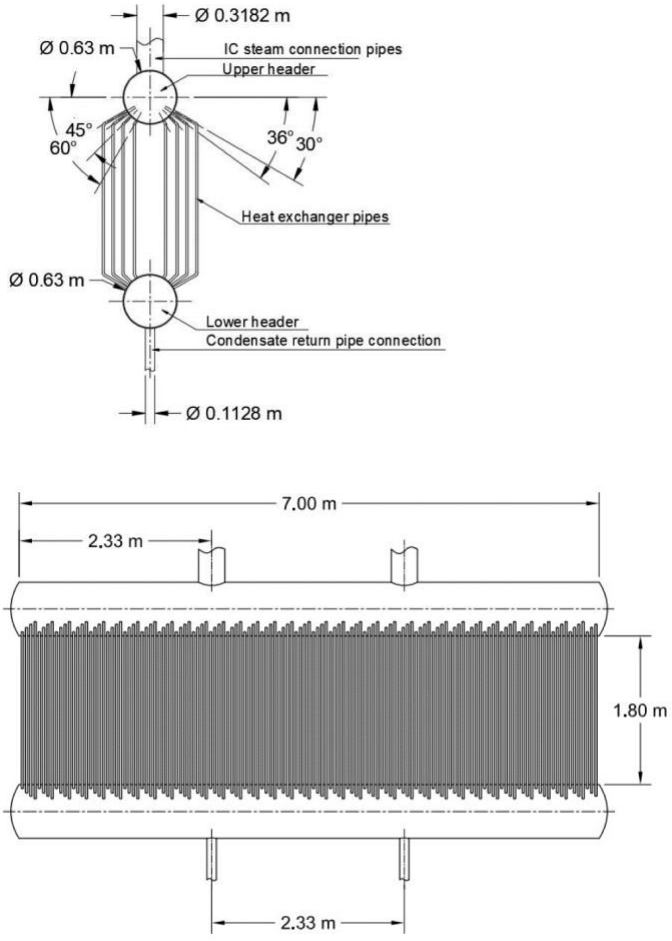

Figure 4. Schematics of the ICS (based on assumptions) (Pomogaev et al., 2022).

3.1.2 Passive Containment Cooling System (PCCS)

The Passive Containment Cooling System (PCCS) also relies on three loops with heat exchangers placed in the containment cavity. The general description (Hitachi, 2023) in §3.6 claims that the system accommodates "*three independent trains*", however §3.6 of the same report and Figure 5 suggest that all three trains are connected to the exact same equipment pool next to the reactor well hence it is difficult to define such redundancy within the PCCS. The purpose of the system is to maintain containment pressure and temperature below design limits during accident scenarios or loss of active containment cooling. During normal operation the system is in a ready stand-by state, filled with water. Since there are no isolation valves between the HEXs and the containment there is no need for trips nor actuators. Even though the system is active during normal operation, it does not transfer notable heat to the equipment pool since the containment temperature is controlled by the Containment Cooling System (CCS). The natural circulation can be initiated by e.g. a pipe break as steam enters the containment, heating up the coolant in the HEX tubes. It is worth nothing that ref. (Hitachi, 2023) postulates in its §3.6 that the PCCS would operate in a single-phase regime during an accident, nonetheless this claim is not supported by the referred material in terms of empirical data.

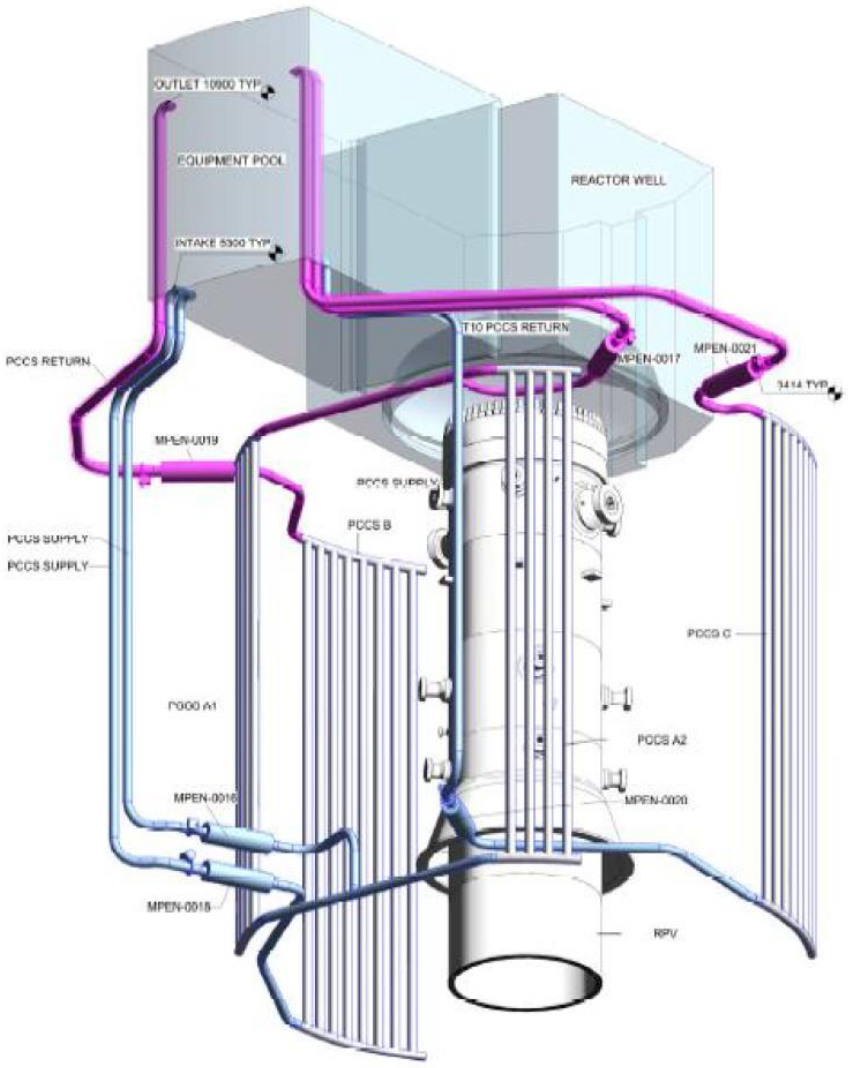

Figure 5. PCCS layout (Hitachi, 2023).

3.2 Relevant experimental facilities

This chapter describes relevant test rigs with respect to the given PSSs whilst also referencing various validation and experimental activities.

3.2.1 PERSEO (OECD/NEA/CSNI/WGAMA benchmark) (Mascari et al. 2023; Narcisi et al., 2021)

The in-Pool Energy Removal System for Emergency Operation (PERSEO) facility is a full-scale separate effect test facility, designed for the development of passive heat removal systems (Mascari et al. 2023). The test loop consists of a pressure vessel, steam and condensate lines, and in-pool heat exchanger (HX), the HX pool (HXP), a steam duct and another pool (OP), the schematics are given in Figure 6. There is no direct scaling ratio between the components of PERSEO and e.g. the isolation condenser of large BWRs, nonetheless the demonstrated phenomena resemble fairly similar topologies.

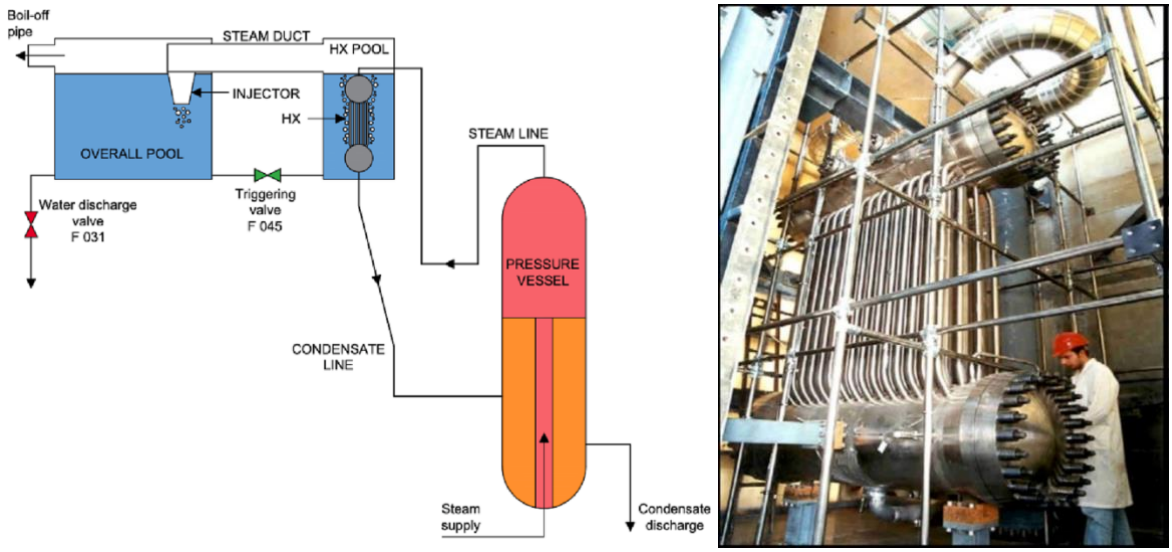

Figure 6. The schematic view of the PERSEO facility (left) and HX (right) (Mascari et al. 2023) ©ENEA.

Ref. (Mascari et al. 2023) disseminates the results of test #7 of the experimental matrix, focusing on system stability and operation during long-term cooling at nominal 70 bar[4] system pressure. The test comprised two parts: (1) verification of system behaviour at 1.4 m and 3.5 m HXP level and (2) verification of the long-term cooling capability without modifying the HXP level while draining manually the OP (simulating the depletion of OP inventory due to the evaporation induced by the heat exchanger). In the end 12 data packages were submitted by 11 organizations representing a variety of lumped-parameter codes and modelling approaches. In terms of exchanged heat, the results showed large scattering and high-amplitude oscillations, within an approximately ± 20 % bound (see Figure 7). Nevertheless, collapsed water levels in the HXP were captured quantitatively as well with minor discrepancies in some cases (see Figure 8). This means that on average the deposited energy (integral power) was still in good agreement with the experiment i.e. the power oscillations did not have a detrimental effect on HXP inventory. Looking at the HXP behaviour from the point of its temperature distribution,

[4] BWRX-300 nominal primary pressure is 72 bar.

the picture is more complicated. Temperature measurements located at the bottom of the pool showed good agreement with calculated trends, meaning that the evolving flow pattern did not have a strong impact on this water layer. On the contrary, midplane and top-plane thermocouple measurements showed larger deviations compared to code results, in both cases system codes tended to overestimate the local temperature meaning that circulation might have been overestimated. Regardless of the spatial discretization of the HXP (1D, quasi-2D, 3D) the thermal stratification of the pool was the most challenging aspect of the passive system's operation, Figure 9 highlights over 50 °C differences in the benchmark.

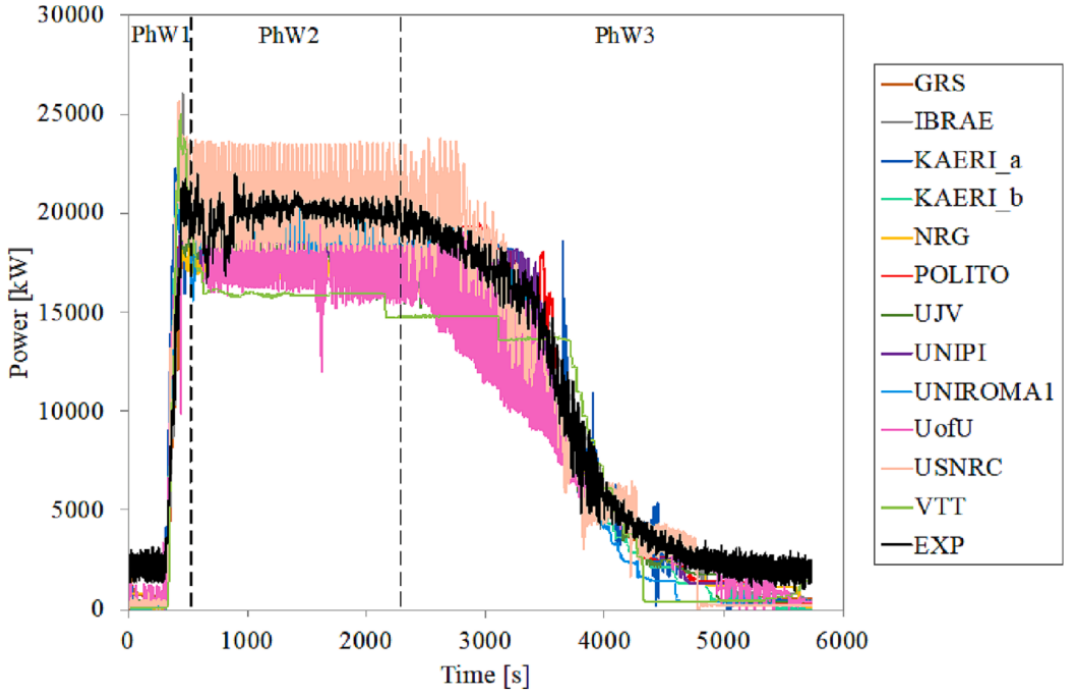

Figure 7. Passive HX power during test #7 (Mascari et al. 2023).

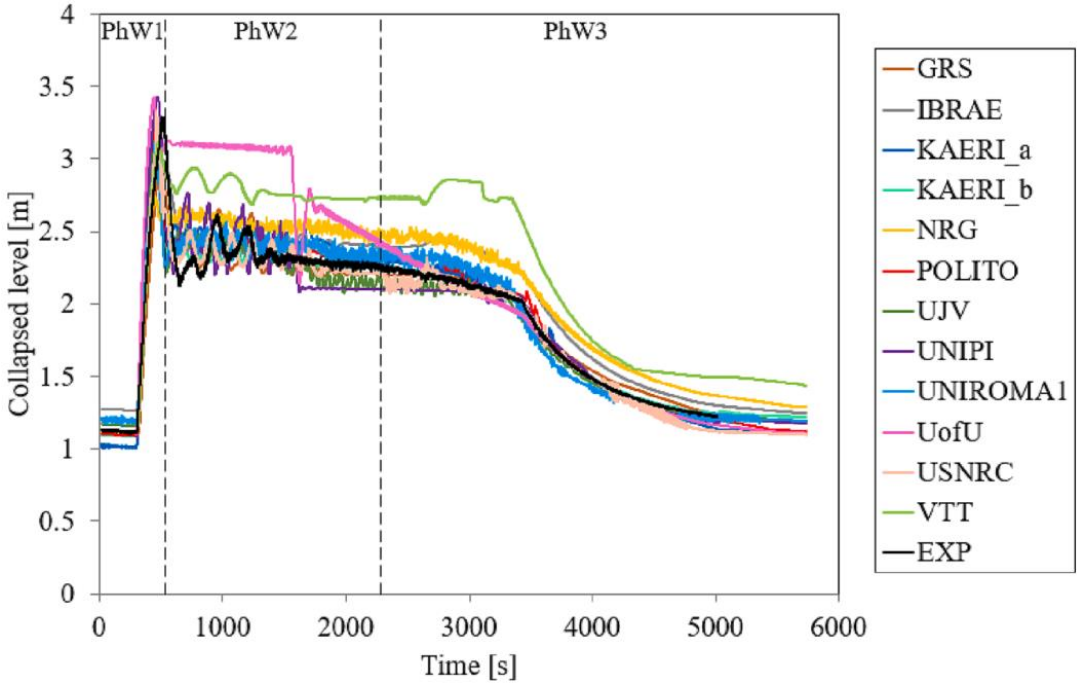

Figure 8. Collapsed water level of the HXP during test #7 (Mascari et al. 2023).

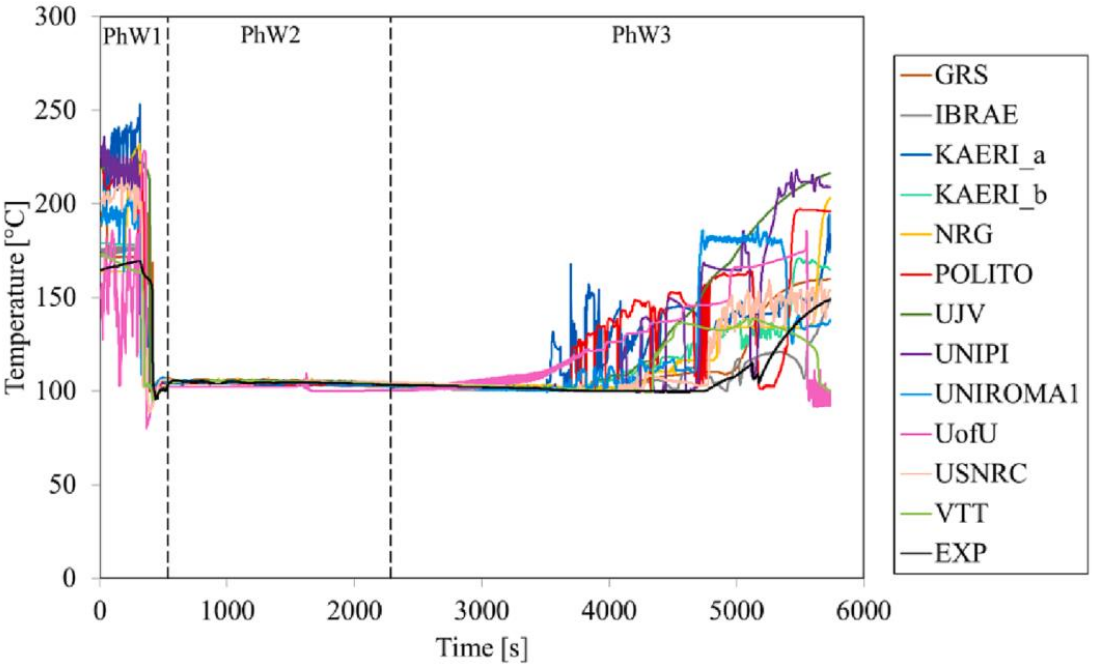

Figure 9. Measured (T-QO034) and calculated temperatures in the midplane of the HXP (Mascari et al. 2023).

Narcisi et al. (2021) utilized part 2 of test #7 measurement data to update RELAP5/Mod3.3 capabilities with respect to nucleate boiling in the pool and film condensation in vertical tubes. By default, the contribution of nucleate boiling is evaluated by[5] the Forster & Zuber correlation with Chen's formulation for the HTC. In the proposed methodology the Chen equation is replaced by Cooper's formula, accounting for parameters e.g. surface roughness, operating pressure and fluid properties. Concerning film condensation in vertical tubes, the default approach is to take the HTC as the maximum of the Nusselt and Shah (1979) values[6]. The improved algorithm includes Kutateladze's method to evaluate HTC in laminar wavy condensation[7] while updating the Shah correlation with the most recent formulation (2009).

Collapsed water levels in the HXP and OP are compared in Figure 10 denoting the default and modified code results along with experimental measurements. There is a slight deviation between the different code versions for OP level but there was significant improvement considering the HXP behaviour. The updated code predicted HX power much better than the default version resulting in higher primary side (SG) mass flow rates. Regarding the boiling heat transfer, the outer surface temperature readings of the tubes showed good agreement with the modified code, besides the expected oscillations due to two-phase flow. Yet the default code overestimated the wall temperatures by ~40 °C due to the underestimation of heat transfer rates in both boiling and condensation. The greatest improvement was observed in terms of pool-side HTC where the updated code predicted one order of magnitude higher HTCs than the default version (see Figure 11). As for the condensation in the tubes the modified version gave HTCs almost twice as high as the default variant, this can be explained by the different predicted heat transfer modes; the default giving laminar condensation and the updated showing wavy laminar condensation.

[5] In Apros the HTC is using the max (Nu) from Dittus & Boelter and 3.66 if the wall temperature is below or equal to the saturation temperature. Otherwise, the max (Nu) is obtained from Dittus & Boelter and the Thom correlation.
[6] Apros is using the old formula from 1979.
[7] In Apros there is no wavy condensation model, only for stratified flow.

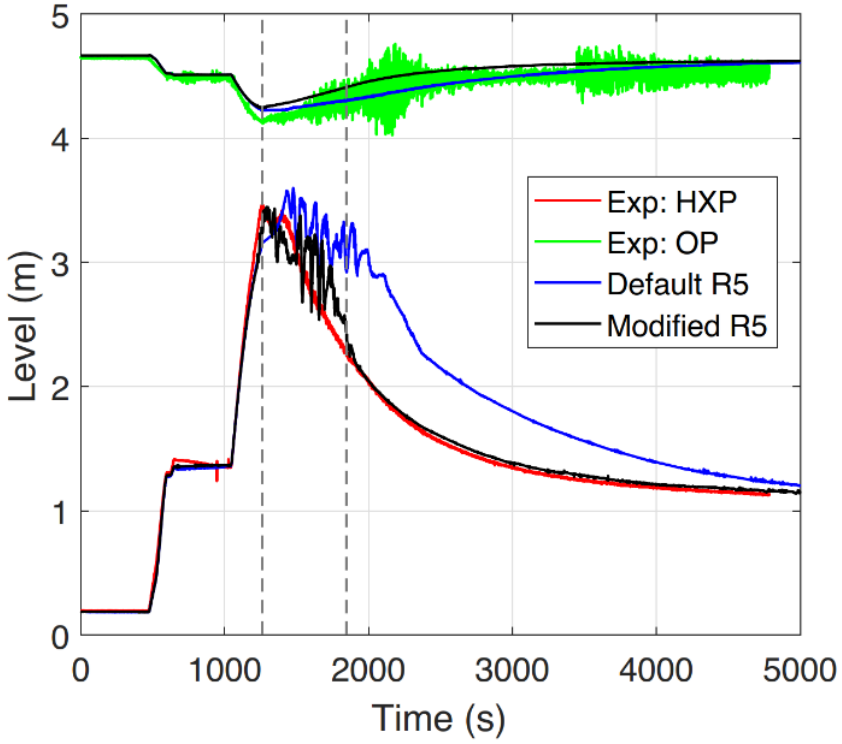

Figure 10. Collapsed water levels in the HXP and OP (Narcisi et al., 2021).

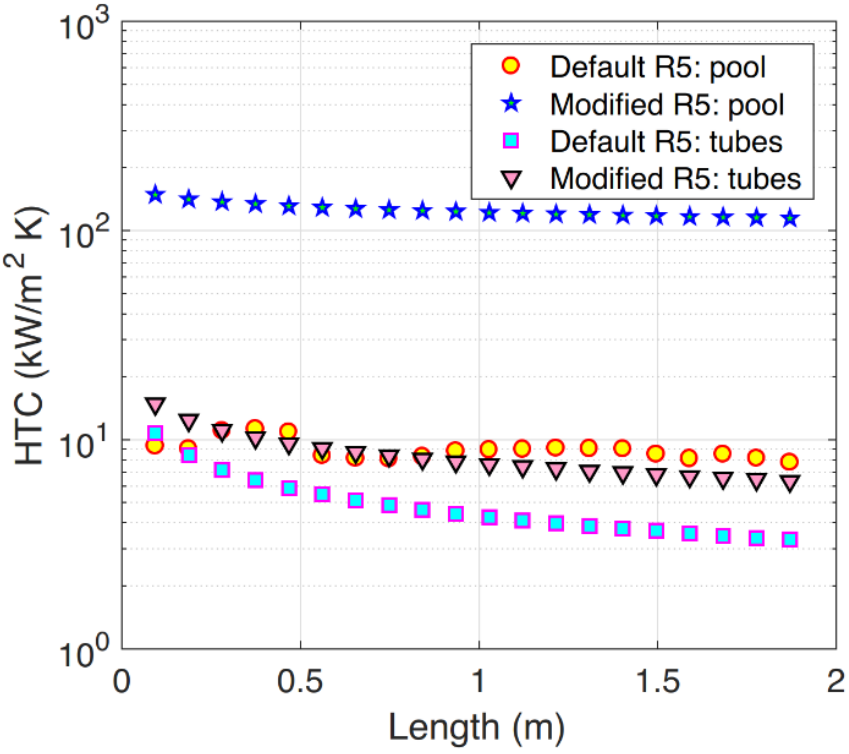

Figure 11. HTCs on HX tube surfaces (Narcisi et al., 2021).

3.2.2 ATLAS-PAFS facility (Jeon et al., 2013; Jeon et al., 2015; Lee et al., 2024)

Extensive code validation efforts have been carried out by Korean affiliates, utilizing data from the PAFS Condensing Heat Removal Assessment Loop (PASCAL) experimental campaign. The test rig was designed and commissioned by the Korea Atomic Energy Research Institute

(KAERI) as part of the ATLAS loop which is the integral test facility of the APR+/APR1400 units. The Passive Auxiliary Feedwater System (PAFS) section consists of a heater, SG, steam and return lines, valves, and the Passive Condensation Heat Exchanger Tank (PCCT). The PCCT contains the Passive Condensation Heat Exchanger (PCHX) which is a horizontally inclined U-tube device. The schematic diagram of the facility is depicted in Figure 12 while the PCHX is illustrated in Figure 13 below. Direction (1) denotes the lateral flow while direction (2) refers to the vertical flow in Figure 13. Initially it was assumed that dominant lateral flows might be associated with stronger bundle-effect while dominant vertical flows would result in weaker bundle-effect.

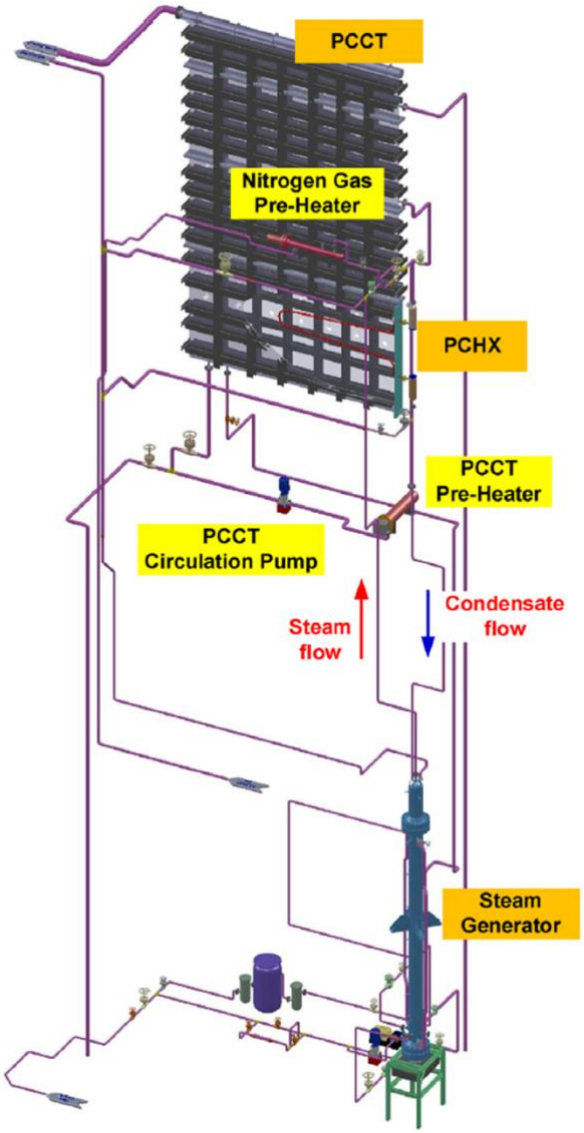

Figure 12. The ATLAS-PAFS facility (Jeon et al., 2013).

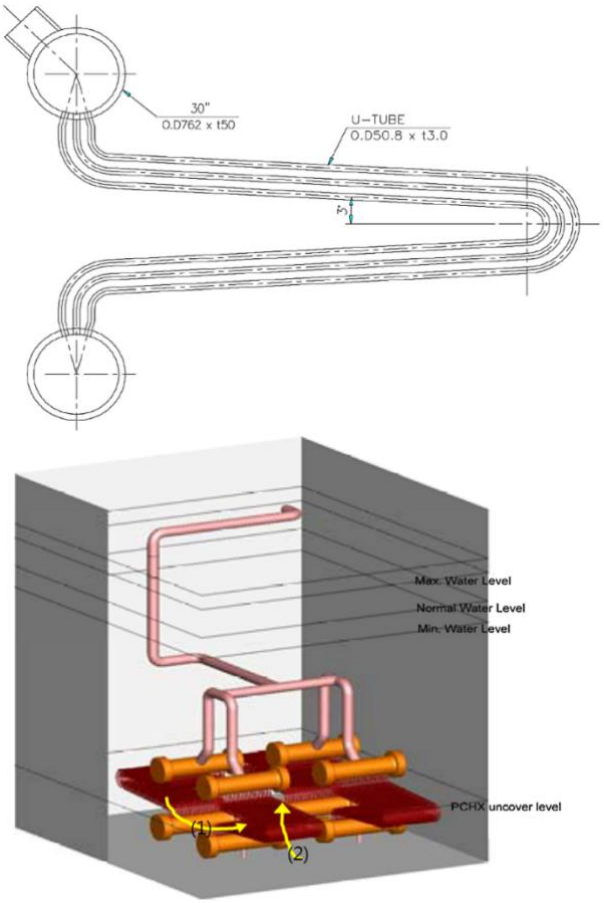

Figure 13. PCHX cross section (left) and arrangement in the PCCT (Jeon et al., 2013).

The operating scheme of the facility is as follows; the SG produces fresh steam which is transferred to the PCHX via the steam line. After condensing in the PCHX the fresh saturated liquid is delivered to the SG inlet by the return line constituting one full cycle.

In ref. (Lee et al., 2024) the authors validated the MARS-KS code using three quasi-steady states, achieved at various power levels to study the behaviour of the PCHX. It has to be noted that in all of these cases fully turbulent natural circulation was observed i.e. the impact of Re on pressure losses was negligible, moreover, the steam and return lines showed single-phase flows thus the uncertainty of wall friction due to two-phase flow could be omitted. Under these conditions the two main driving factors behind the natural circulation were (1) the SG power and (2) the pressure losses. Since orifices represented the largest hydraulic resistance their effect on the PAFS performance was deemed to be great, hence subsequent studies focused on the orifice diameter ratio ($\beta = D_{orif}/D_{pipe}$).

It was found that with too little ratios ($\beta \leq 0.5$) the pressure losses were overestimated resulting in low flow rates. With larger ratios ($\beta \geq 0.75$) the pressures were lower resulting in higher flow rates. In simulations using smaller ratios the SG pressures did not vary significantly as the heating power was increased (300-540-750 kWe), nonetheless, as power and steam flow rates increased the orifice Δp also increased due to their relationship with the flow rate.

The main findings of the study were summarized as:

- Engineering artifacts with relatively large pressure drops should be considered carefully in the model, more detailed depiction is recommended.

- Since $\Delta p \propto m^2$ the effect of losses will vary depending on the operating conditions.
- As the $\Delta p \propto 1/\rho$ the device that causes a relatively large pressure drop will have a greater impact on the steam line compared to the return line.

Figure 14 depicts the impact of β in terms of SG pressures and fresh steam mass flow rates. Reiterating earlier considerations, the higher the pressure the lower the mass flow rate, discrepancies between thermal-hydraulic parameters showed a positive correlation with SG power.

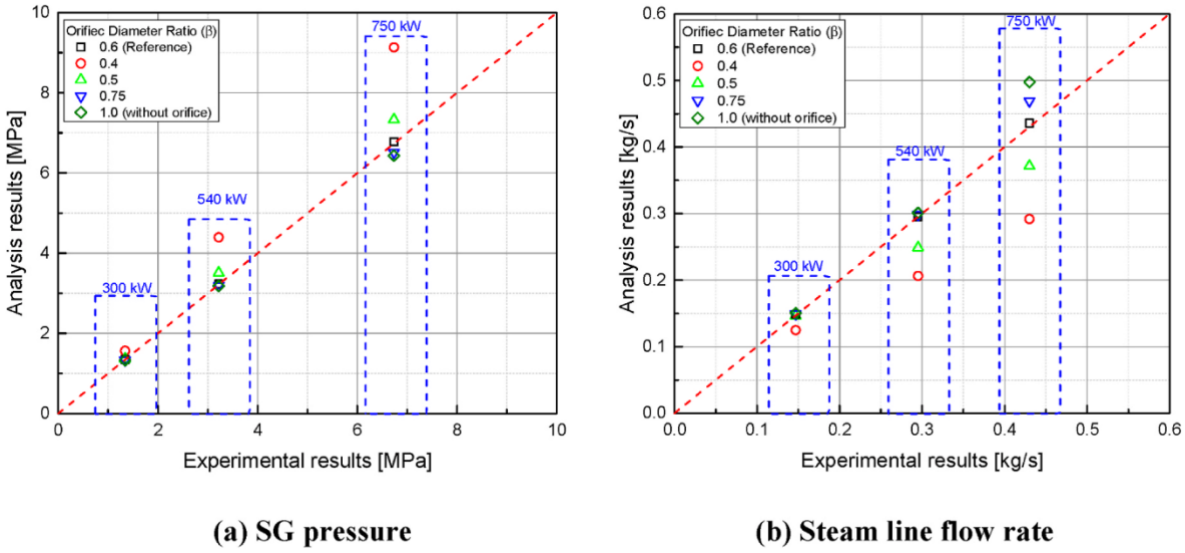

Figure 14. Pressure and steam mass flow rate comparison in PASCAL experiments (Lee et al., 2024).

Ref. (Jeon et al., 2013) used the same quasi-steady state PASCAL experiments putting the emphasis on the modelling of the PCHX using the MARS-KS system code. Experimental and analytical local heat transfer coefficients (HTCs) were compared from the steam region, considering various empirical formulae (19 models) e.g. Shah, Chen, Thom, etc. The HTC distribution of the bottom part of the inclined U-tubes was captured quantitatively well even though the profiles showed noticeable dispersion. On the other hand, HTCs in the upper part posed challenges for all applied models, generally HTCs were underestimated by the formulae at each power level. Flow regimes were identified as annular in the ~2 m inlet section and stratified beyond, hence the study focused on the annular region, but the importance of annular-stratified transition was also highlighted. In the end the combination of the Dobson & Chato (1998) for annular and Cavallini et al. (2006) for the stratified region was identified as the optimal set of equations to describe the PCHX behaviour (Jeon et al., 2013). Even this best-estimate approach could not capture the HTC distribution in the upper section of the heat exchanger tubes meaning that the applied models were missing some local phenomenon (see Figure 15).

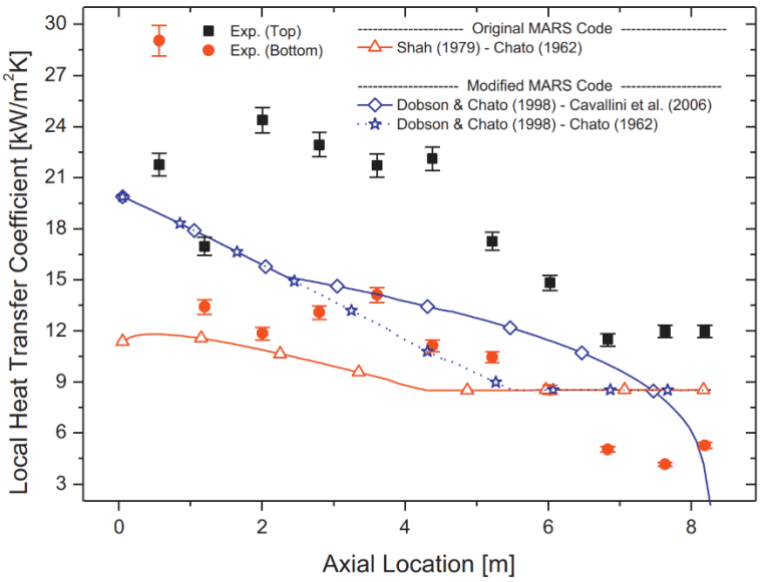

Figure 15. SS-300-P1 test results at 300 kW heater power (Jeon et al., 2013).

Ref. (Jeon et al., 2015) shed some light on such phenomenon and tackled the issue from the pool side, concerning nucleate boiling on the outer surface of the PCHX tubes. As one can expect the PCHX induces nucleate boiling on the pool side, however the boiling is heavily dependent on the location of a given tube. The lower section of the HX is unaffected by the upper section however, the upper section is influenced by the boiling in the lower section. This influence appears in the form of gravity/buoyancy induced natural convection, as the PCCT water level decreases, bubble generation intensifies, reducing the tube-water interfacial area for the upper section. As power levels (steam flow rates) increase the turbulence around the upper U-tubes also grows further enhancing heat transfer on the affected tubes compared to the lower part. Figure 16 shows the mechanism which means that the two sections of the PCHX demonstrate different behaviour.

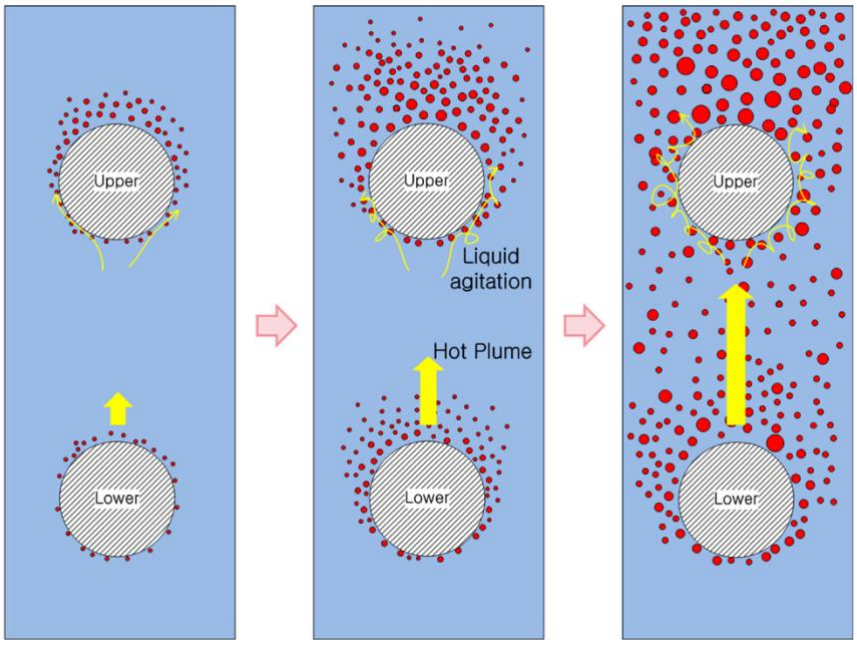

Figure 16. Heat transfer mechanisms on the external surface of submerged tubes (Jeon et al., 2015).

Since the nucleate boiling is governed by subcooled pool boiling and subcooled forced convective boiling the study adopted new correlations for the different tube sections. The default Cornwell & Houston (1994) saturated pool boiling correlation slightly over-predicted HTCs with higher PCCT water levels (within a ± 20 % bound), since the formula ignored the relatively high ~13 K subcooling. A suppression term (S) was borrowed from the Shah (2005) correlation by non-dimensionalizing the degree of subcooling with the wall superheating.

For the upper part of the tubes a Chen-type correlation was developed due to its reasonable performance with horizontal tubes. Under high PCCT water level (9 m) the Chen (1966), Polley et al. (1980) and Cornwell-Houston (1964) correlations all gave quantitatively reasonable HTC profiles, slightly underestimating and overestimating values in the upper and lower parts, respectively. At low PCCT water level (4 m) these formulae clearly underpredicted HTCs in the upper section of the PCHX underlining the differences in heat transfer mechanisms. The new correlation aimed to consider the multi-dimensional flow pattern in the pool, this was achieved by averaging the liquid HTC in the parallel and perpendicular directions to the tubes. Using Kutateladze's method, the square root of the sum of the squares, the liquid HTC (h_l) was weighted towards the larger HTC.

In this study the Whitaker (1972) and Dittus & Boelter (1930) equations were used for cross and parallel HTCs. Due to the turbulence and motion, created by the bubble formation over the lower tubes, the single-phase liquid HTC is enhanced over the upper tubes. This effect was taken into account by the enhancement factor (F), derived from the equation of Polley et al. (1980).

The new approach showed clear improvement compared to the default Chen (1966) correlation as shown in Figure 17. Looking at 288 data points from the three PASCAL experiments the mean deviation was 7.9 %, combining this database with 78 data points from ATLAS-PAFS experiments only 7 out of 366 data points had deviations greater than 20 %.

In conclusion, 15 correlations were tested, none of them could be generally applied to the lower and upper sections of the HX, the phenomenological differences in heat transfer mechanisms were too great for these formulae. One has to consider the flow patterns and the bubbling in such correlations. It is worth noting that the proposed model is heavily fitted for the given facility i.e. even the more universal description of the phenomena has its limitations.

Despite the engineering assumptions concerning lateral-vertical flow patterns, it was shown that the bundle effect cannot be neglected even in a vertical-dominant velocity space, especially under boiling. Even though these observations were based on a slightly inclined ($\theta = 3°$) horizontal passive heat exchanger, the implications regarding tube-interaction and 3D flow patterns are important also for vertical heat exchangers, as for their collectors. For such HXs, the larger the tube bank the larger the difference in heat transfer mechanism in the radial direction. Inner tubes are more affected by the flow pattern/boiling regime in the lower section of the heated length while outer tubes are less exposed to lateral (cross) flows involving the pool inventory. These characteristics are heavily dependent on the layout of the heat exchanger, e.g. pitch, number of tubes, size of the surrounding water volume and so on.

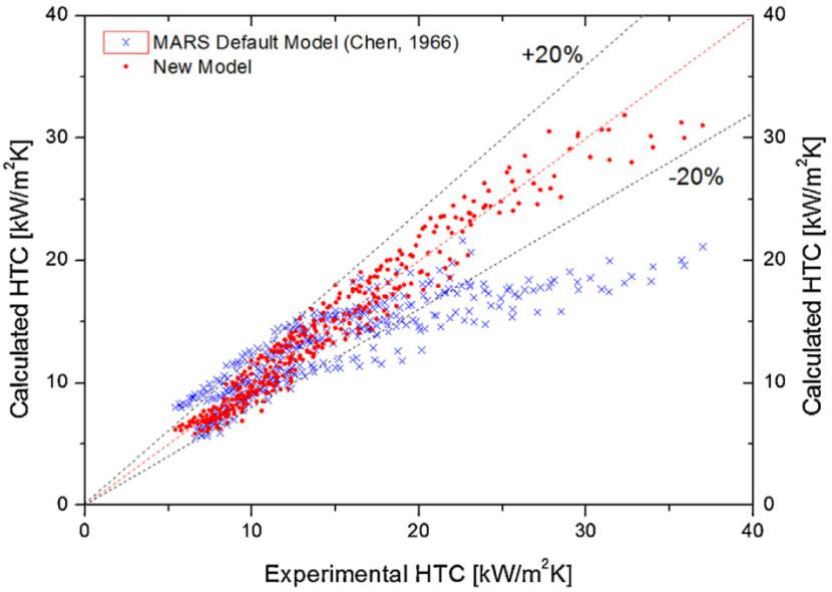

Figure 17. Default and modified nucleate boiling models' performance (Jeon et al., 2015).

3.2.3 PANDA facility (Kapulla et al., 2022; Paladino et al., 2022; Paranjape et al., 2024)

The PANDA facility (Passive Nachzerfallswärmeabfuhr und Druck-Abbau Testanlage) is a large-scale, multi-compartment test facility, designed to represent the SBWR/ESBWR containments. Power and volumes were scaled 1:40 while pressure, relevant heights and pressure drops are 1:1. The rig consists of six large vessels, representing the various containment compartments. The non-nuclear RPV houses 115 electrical heaters, placed in a shroud which simulates the riser, enabling natural circulation within the vessel. Two main steam lines (MSLs) deliver the fresh steam to the two drywell (DW) vessels. These tanks are connected to the two slightly larger wet well vessels (WW) or suppression chambers. The last vessel is the Gravity Driven Cooling System (GDCS) which can function as an additional containment volume for WW gas space. The four rectangular pools above the DWs are dedicated to three passive containment coolers (PCCs) and one isolation condenser (IC). One PCC is connected to DW1 while two PCCs can cool DW2. Figure 18 depicts the view of the facility with its main components and the cooler triplet using during the H2P6 tests in one of the DWs (HYMERES-2 project). The main parameters of the facility are summarized in Table 3.

Table 3. Main parameters of the PANDA facility (Lübbesmeyer&Aksan, 2003; Paladino et al., 2023).

Parameter	Value
Facility total height [m]	25.00
DW/WW vessel midplane diameter [m]	4.00
DW height [m]	8.00
DW volume [m^3]	89.90
WW height [m]	10.11
WW volume [m^3]	115.90
GDCS height [m]	6.06
GCS volume [m^3]	17.60
Total volume of 6 vessels [m^3]	515
Max. electrical power [MWe]	1.5
System pressure [bar]	0.2-10.0

Parameter	Value
System max. temperature [°C]	200

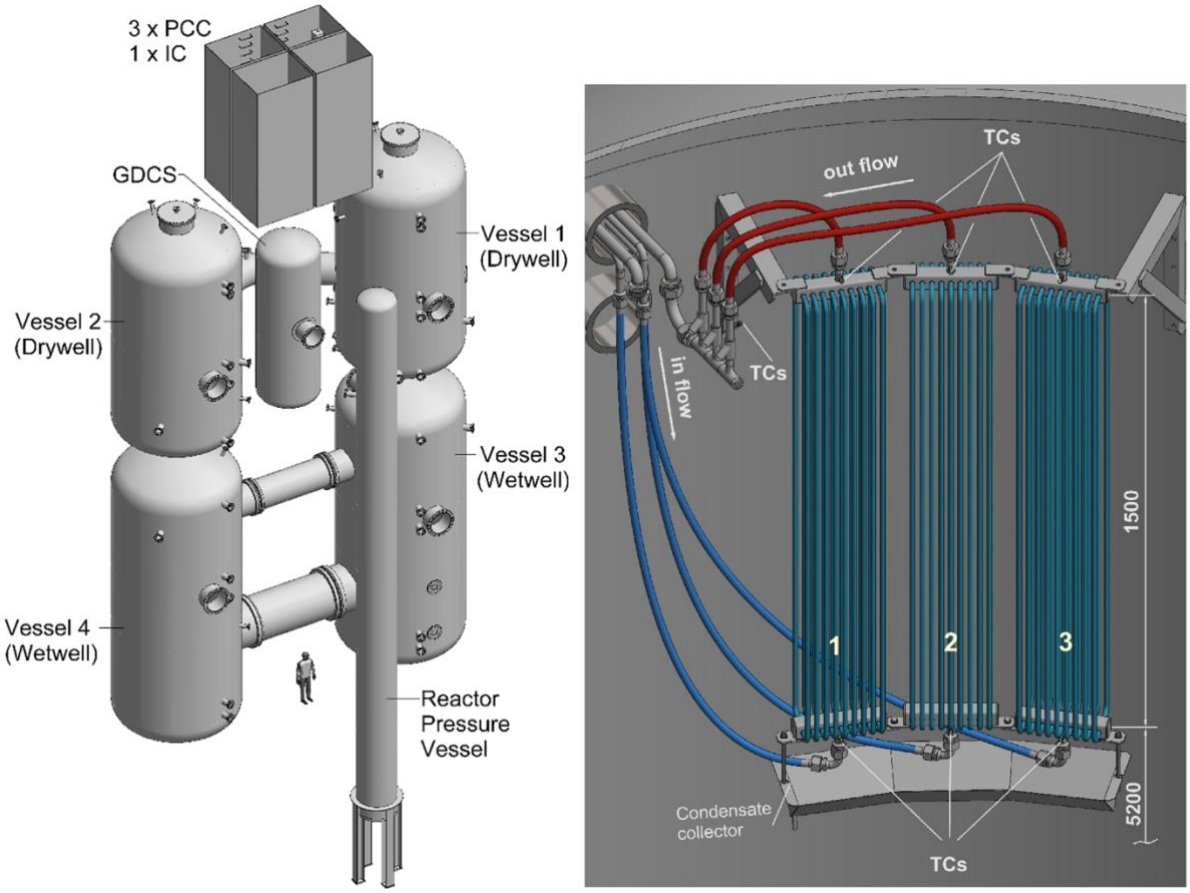

Figure 18. PANDA facility bird's eye-view (left) and safety condensers in the DW (right) (Kapulla et al., 2022; Paladino et al., 2022).

Ref. (Kapulla et al., 2022) disseminates the experimental and subsequent modelling results of the H2P6 campaign within the OECD/NEA HYMERES-2 project. The test series comprised two experiments using three separate coolers mounted in the upper section of a DW (see Figure 18). Prior to both tests the DW was preconditioned with a gas mixture of 40/60 % air/steam before the helium plug could build up in the upper section of the vessel (Kapulla et al., 2022). For experiment H2P6_1 all three coolers were operating while for H2P6_2 only one cooler was available. After preconditioning, forming the He layer and a 390 s relaxation period the cooler(s) activated with a 0.5 kg/s fresh coolant flow, thereafter the depressurization was performed for 4500 and 13500 s, respectively, depending on the number of active coolers. Due thermohydraulic and structural similarities the ΔT values of the coolers were practically identical hence the average ΔT represented the characteristic decay of the extracted heat. Figure 19 describes three distinct periods with normalized time axis ($t = t_{max}/t_{exp}$):

- period 1: $0 < t < 0.46$ - the coolers affect the upper half of the vessel
- period 2: $0.46 < t < 0.67$ – recovery of heat removal capacity
- period 3: $0.67 < t < 3.0$ - the entire volume is participating in the mixing

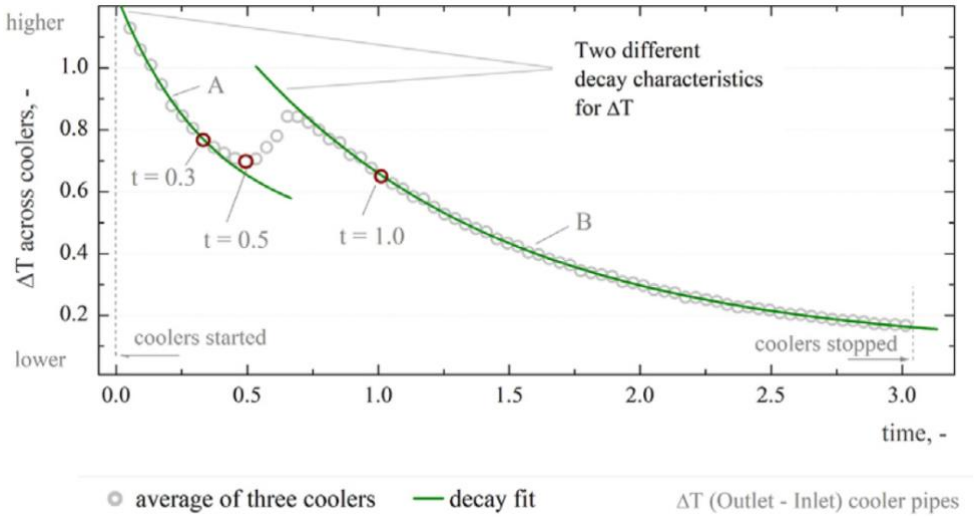

Figure 19. Mean $\boldsymbol{\Delta T}$ trends during H2P6_1 (Kapulla et al., 2022).

During the first period the coolers could affect only a smaller, confined section of the total volume where the induced natural circulation could result in a more effective cooling. This initial strong separation between the lower and upper parts of the DW atmosphere was broken at the onset of the recovery phase as the cold region (cooler's location) started to descend into the lower volume. Subsequently the atmosphere in the vicinity of the coolers mixed with the warmer atmosphere in the lower section, altering the composition of the gas that the coolers interacted with. Most probably this effect increased the HTCs temporarily along the coolers for a brief episode (period 2). As the flow spread across the whole volume in period 3 the temperature decay slowed down as more warm gas met the coolers. Figure 20 illustrates the temperature profiles for the three periods of H2P6_1.

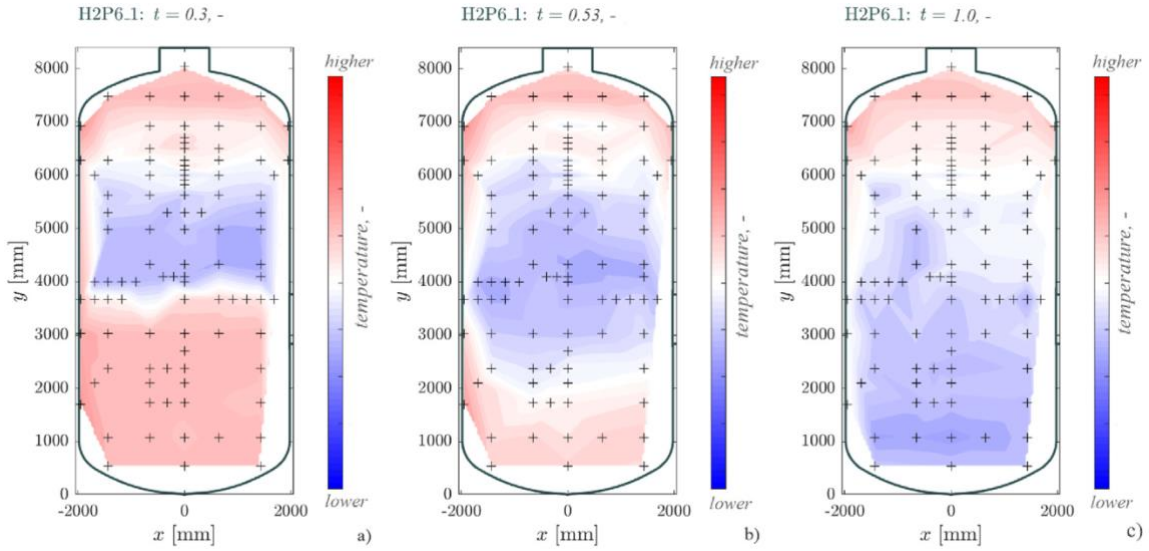

Figure 20. 2D DW gas temperature profiles during the H2P6_1 test (Kapulla et al., 2022).

Concerning H2P6_2, the non-dimensional ΔT trends were compared using inverse time scaling meaning that the number of coolers was inversely proportionate to the length of the transient. In Figure 21 the decay curves collapse which indicates that the physics behind the different periods do not change depending on the number of coolers. Correspondingly similar behaviour was seen regarding helium concentrations as well, the non-condensable distribution followed

the same topology in both cases. In other words, the effect of utilizing three coolers instead of a single unit is simply additive.

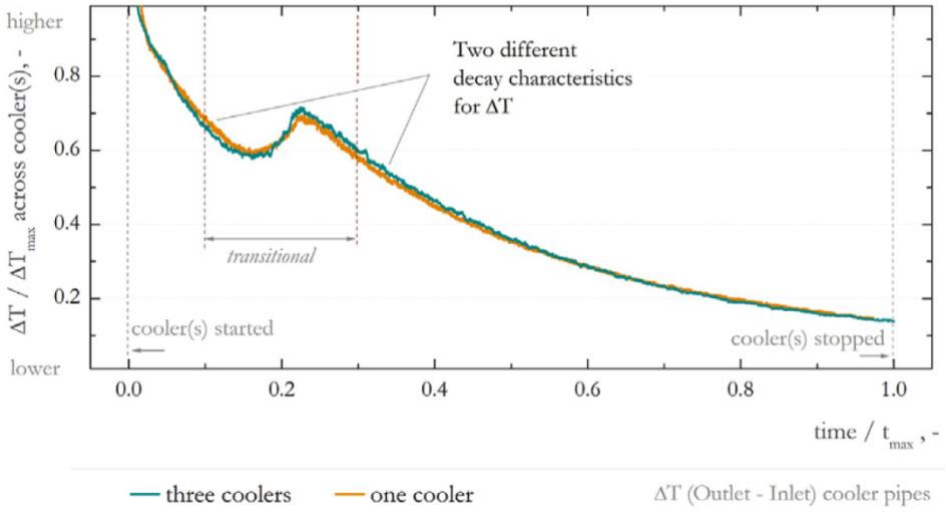

Figure 21. Temperature differences with one and three coolers (Kapulla et al., 2022).

Ref. (Paladino et al., 2022) shared the results of various PANDA experimental series, for the sake of brevity this excerpt will focus on §3.3.2. H2P4 series, the task dedicated to BWR containment operation with and without spray injection. Spray and sparger lines were installed in vessel 3 (WW) for the sake of the experiments as illustrated in Figure 22. The experiment entailed four phases:

1. steam injection into the suppression pool via the sparger
2. no injection, configuring the facility for the following phase
3. spray water injection
4. continued data acquisition without injection

The main objective of H2P4 was to find a relationship between the reduction of the heat-sink capability of the suppression pool (WW) due to the formation and stability of thermal-stratification during the venting process, and the containment pressurization history. The sparger submergence was 1.2 m for H2P4_2 while 0.5 m in H2P4_3. The air plug in vessel 3 was pressurized to 2.0 bar prior to the tests (with air) while the steam flow rate in the sparger was 180 g/s, for both tests the target plug pressure was 3.4 bar. During phase 1 a sharp thermocline developed in both cases, affected by the given sparger submergence, the temperature difference across this zone was 112 °C. It is worth noting that the thermocline did not move downwards in the water volume during the time of the experiments indicating very weak natural circulation. In phase 3 the spray initiated the depressurization, despite an initial cooling of the gas plug the stratified temperature profile remained intact. Reaching the mentioned target pressure took 21386 s (5.9 hrs) and 13872 s (3.9 hrs) for H2P4_2 and H2P4_3, respectively. The large difference arose from the sparger configuration where in former case the steam had to traverse a much higher water column before reaching the void above the water which ultimately led to more intense interfacial heat transfer i.e. slower pressurization compared to the latter case.

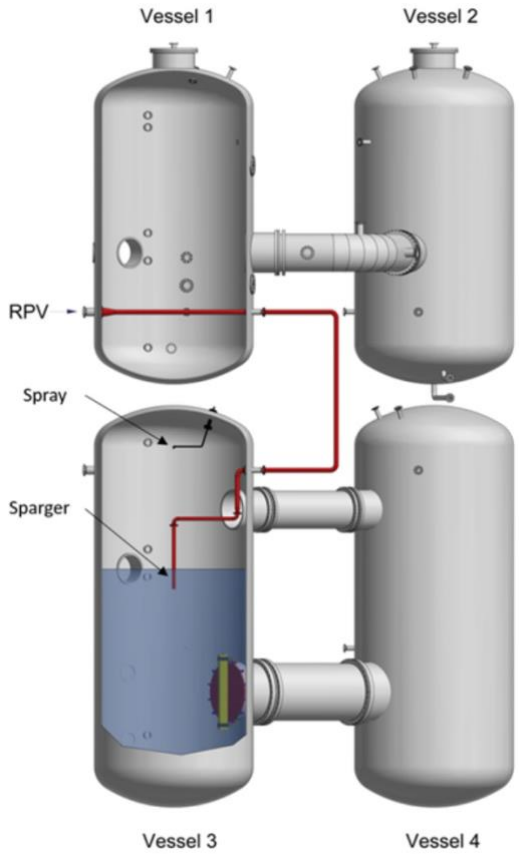

Figure 22. PANDA facility modifications for H2P4 tests (Paladino et al., 2022).

Figure 23 demonstrates the thermocline during phase 1 and the impact of spray injection during phase 4. Despite the large temperature difference between the gas and liquid volumes and a long ~3.5 hr steam injection, the thermocline formed only a relatively thin layer of ~25-30 cm. With regards to the cooling effect the gas plug has not shown significant deviation from the phase 1 end-state with a ~12 °C ΔT reduction in phase 3.

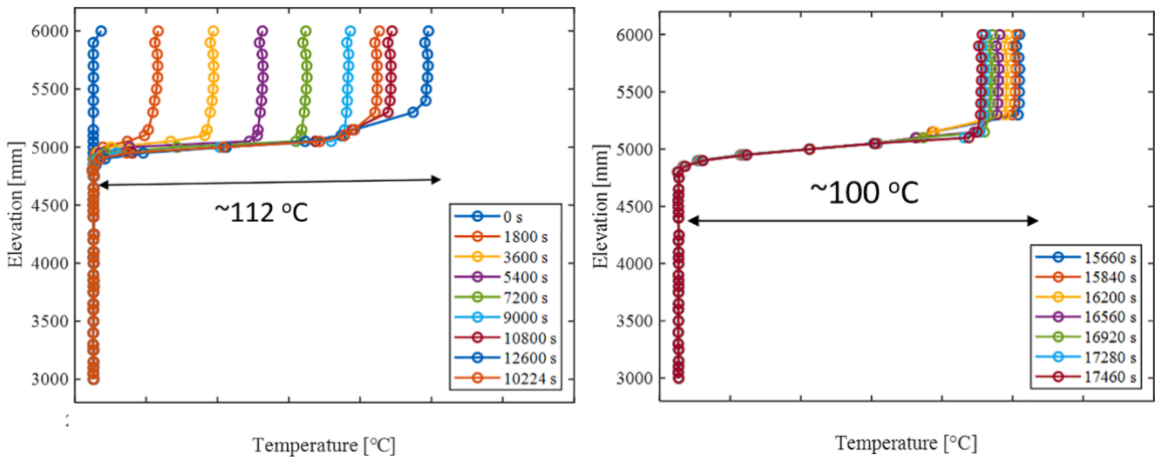

Figure 23. Thermal stratification in the wet well during steam injection (left) and spray injection (right) in H2P4_3 Paladino et al., 2022).

It is worth highlighting that the hereby discussed wet well behaviour does not translate into water wall behaviour i.e. IC pool behaviour unconditionally. In the PANDA cases the water

mass was heated by a single point-source-like injection point whereas in water walls the submerged containment itself induces and supports natural circulation. This induction is a result of a growing heated surface as the containment atmosphere also stratifies as a result of steam ingress (e.g. LOCAs) or passive heat removal system operation (e.g. SBOs). Such mechanisms do invoke a thermocline movement over the course of several days, downwards to the bottom of the water wall as shown in benchmark exercises of the ELSMOR project (Szogradi & Alblouwy, 2025). Postulating a longer sequence of events in ref. (Szogradi & Alblouwy, 2025) it was shown that the initial containment heat-up can induce and promote natural circulation on the water wall side, however as the enthalpy intake of the containment diminishes at some point the water wall starts to cool the containment. After this point the containment-based driving force of the water wall's natural circulation starts to decay, eventually degrading the circulation itself.

4. Modelling of PCCS performance

The principal of the modelling approach was that the whole system behaviour (PCCS water cooling circuit loop including the water pool, and the containment vessel) is simulated with the Apros system code. The OpenFOAM CFD software was applied only for the containment vessel and a vertical part of the PCCS pipe inside the vessel. The inlet water mass flow and temperature of the vertical PCC pipe, as well as the vessel initial pressure and gas temperatures, were calculated with Apros and given as boundary conditions for the OpenFOAM CFD simulation.

The first objectives of the simulation work presented in this report were to build up the preliminary (and simplified) code simulation models for the PANDA test series P1A4, check the usability and accuracy of the models, assess the soundness of the preliminary simulation results, and map the needed improvements of the simulation models for further work.

4.1 Panda experiment P1A4

The selected simulation case was the one series of experiments will be performed in the Panda facility within the OECD/NEA PANDA project in 2025 to study performance of the Passive Containment Cooling Systems (PCCS). The characteristics of the facility are described in section 3.2.3. The test series P1A4 comprises a single-pipe PCCS system inside a PANDA pressure vessel including a water pool. The planned test arrangements is shown in Figure 24. The inside diameter of the PCCS pipe is of the order of 38 mm having a vertical condensation length of 6 m inside the vessel. The pipe distance from the vessel wall is about 1m. The interest phenomena under consideration are steam condensation rate on the outer PCCS tube, natural circulation flows inside the PCC pipe and vessel atmosphere, heat transfer rate through the PCC pipe wall, thermal evolution in the PCC water pool, and mixing/stratification phenomena inside the vessel atmosphere (Rivera et al., 2024). The concept with a single PCC pipe will be used to acquire a high-resolution experimental database of flow data, temperatures, and heat transfer coefficients under LOCA conditions, and to enhance the suitability of the data for the code validation work.

The test series will be also used for organising an OECD/NEA international benchmark exercise in 2025/2026. The steady state (quasi-steady) test will be calculated as a blind calculation, and the transient test as an open post-calculation.

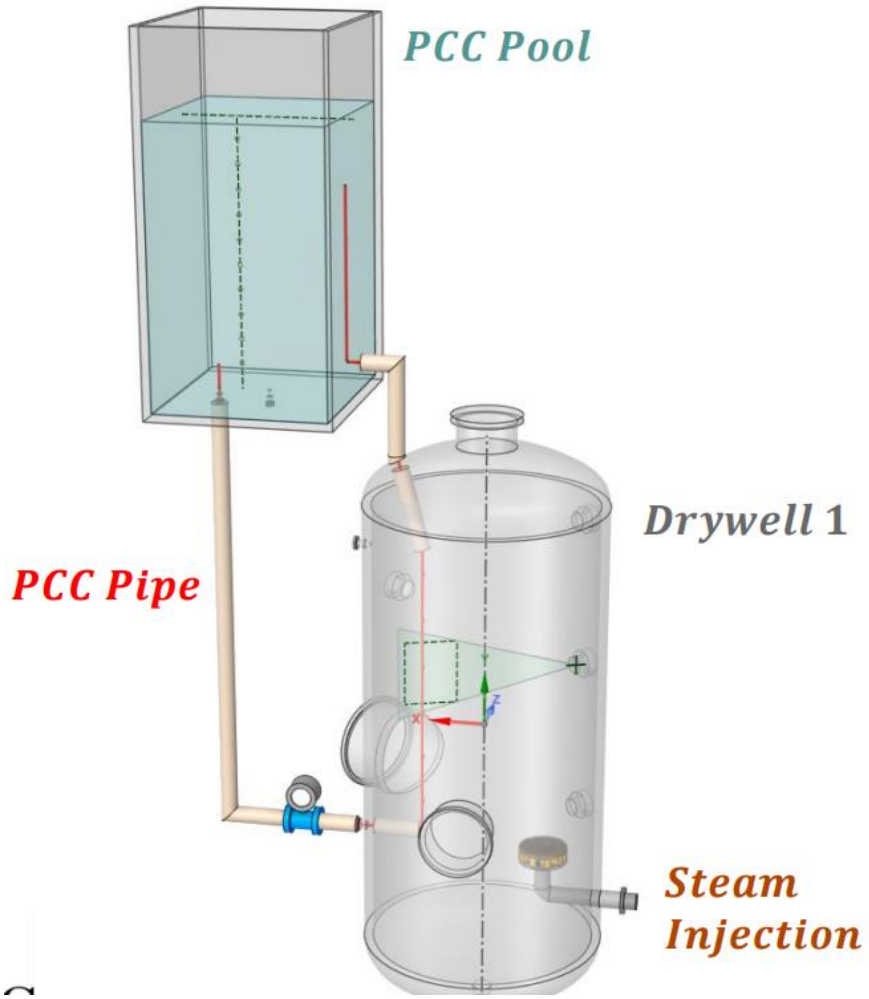

Figure 24. Schematic of the test arrangement of P1A4 test series (Rivera et al., 2024).

4.2 System code modelling with Apros

4.2.1 Model description

The vertical part of the PCC pipe HEX inside the vessel is modelled with eight heat pipe components each of which having three calculational axial nodes (Figure 25).

Apros nodalisation for the containment vessel is shown in Figure 26. The current configuration consisted of 41 containment nodes representing volume sections of the vessel. The model approach was a so-called “pseudo-3D” nodalization, where the containment vessel was divided into 8 horizontal nodes, which were further divided radially (azimuthally) into 5 nodes. The bottom level node was kept as a singular node. The adjacent nodes were connected with gas flow paths. One sump was located in the bottom level node which was a final location of all water condensate from wall condensation. The principle positions of the vertical PCC pipe and the steam injection nozzle are indicated as red and yellow colours in Figure 26. The steam injection was located on the opposite side of the vessel to the PCC pipe location. The wall heat structures and related insulation were also included.

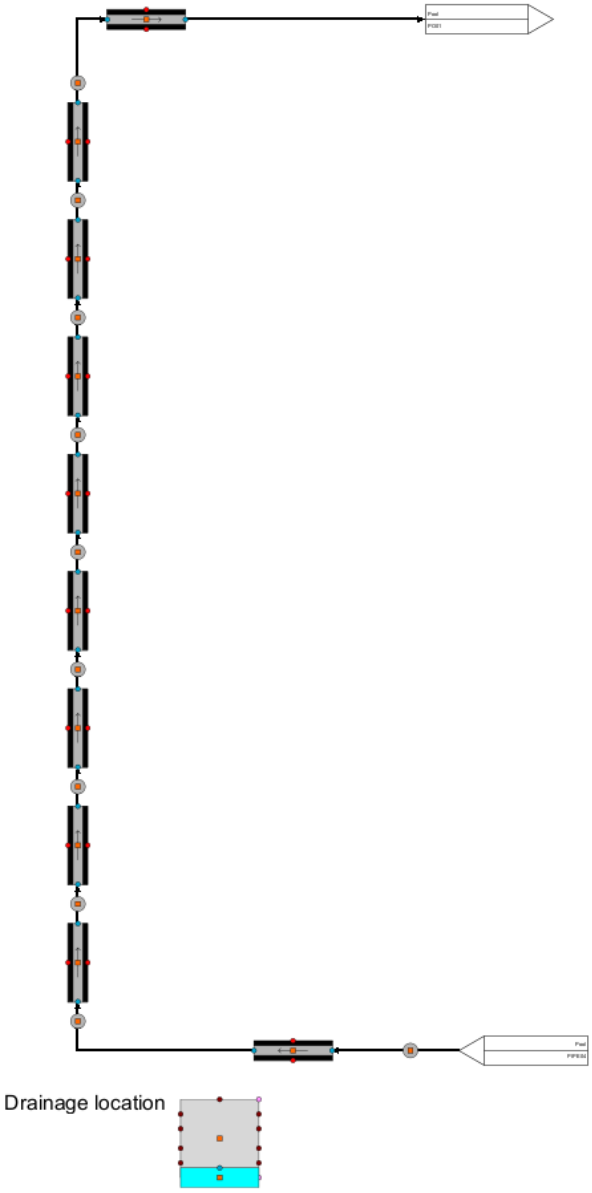

Figure 25. Apros nodalisation for a vertical section of the PCC pipe inside the containment vessel.

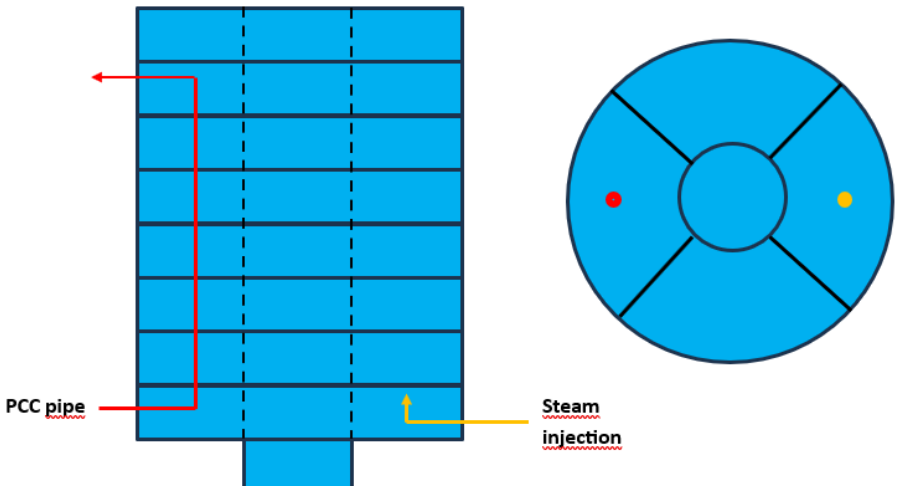

Figure 26. Apros nodalisation for the containment vessel.

Initially, all temperatures, both in the PCCS and the vessel, were assumed to be 20 °C in the simulation. Initial pressure was 1 bar. The vessel atmosphere was assumed to be dry with an infinite small relative humidity. Steam injection pressure and temperature were fixed to 2.5 bar and 130 °C, respectively.

4.2.2 Heat transfer modelling

The heat transfer method in the Apros containment library is based on combined heat and mass transfer calculations based on the mass diffusion theory and Ackermann´s approximate corrections for the heat and mass transfer coefficients (default option) (Silde et al., 2019). Heat transfer between the atmosphere and structures is a sum of sensible and latent heat transfer.

The Apros containment library does not have any specific heat transfer correlation for a single-pipe system. In the case where the shell side of a heat exchanger is in the containment, the Grimison correlation is available in Apros. The correlation is design for a tube bank and the configuration is characterized by information of the tube arrangement, the diameter and the transverse pitch S_T and longitudinal pitch S_L between tube centres (Incropera & DeWitt, 1996).

The Nusselt correlation used is

$$\overline{Nu} = 1.13 \cdot C_1 \cdot \mathrm{Re}_{\max}^{m} \ \mathrm{Pr}^{1/3} \tag{9}$$

where *Re* is the Reynolds number, *Pr* is the Prandtl number C_1 , and *m* are the constants according to tube arrangement (aligned or staggered), tube diameter, and transverse and longitunal pitches between the tubes. Using the heat-mass-transfer analogy, the corresponding Sherwood number is

$$Sh = 1.13 \cdot C_1 \cdot Re^{m} \cdot Sc^{1/3} \tag{10}$$

where *Sc* is the Schmidt number.

The convective heat transfer coefficient is solved from the Nusselt number, and the mass transfer coefficient for the condensation/evaporation processes are solved from the Sherwood number.

Unfortunately, the correlations is designed for a tube bank (not for a single tube) under forced convection conditions. The PANDA test P1A4 will consists of a single pipe PCCS, and hence, the heat and mass transfer correlations are not necessarily directly suitable for this test conditions. However, the correlators are considered to be the most suitable of available Apros correlations and are, therefore, used in this work. In the future work, a more suitable correlation should be selected and implemented in Apros, and the results should be studied and benchmarked with the current correlation result.

4.2.3 Simulation results

4.2.3.1 Null simulation

In the null simulation, all initial temperatures (liquid and gas) were assumed to be 20 °C and there was no steam injection to the containment vessel. Because the vessel atmosphere was initially dry and the temperature difference across the PCC pipe wall was zero, no heat transfer from the vessel to the PCCS system occurs. Therefore, presumably steady state vessel pressure and water mass flow inside the PCCS cooling circuit should be reached. The purpose of the null simulation was to check that the Apros model gets the steady state.

As Figure 27 and Figure 28 show, the model reaches well steady state conditions in the containment vessel.

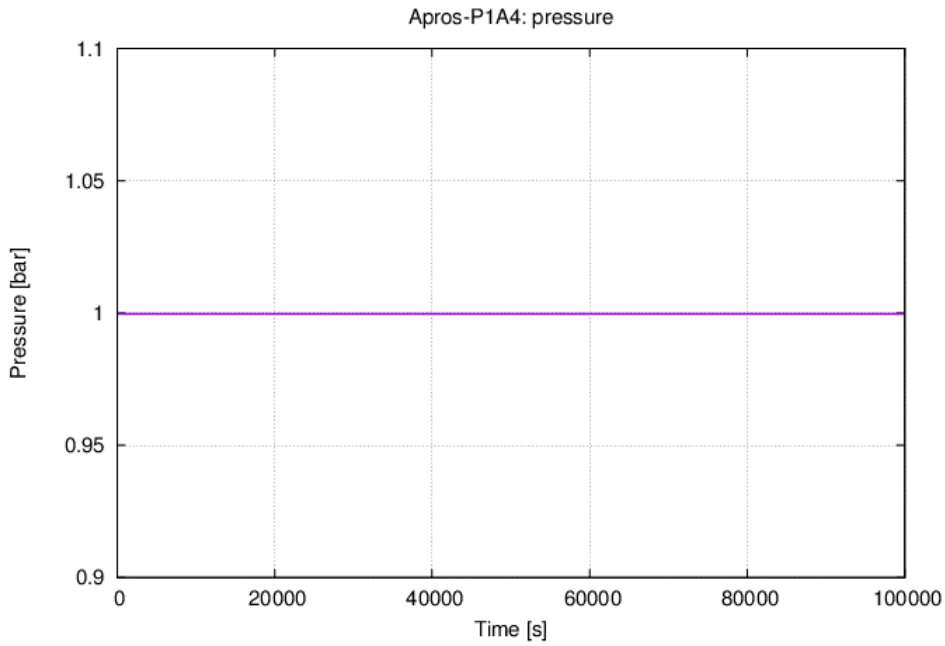

Figure 27. Containment vessel pressure (null simulation).

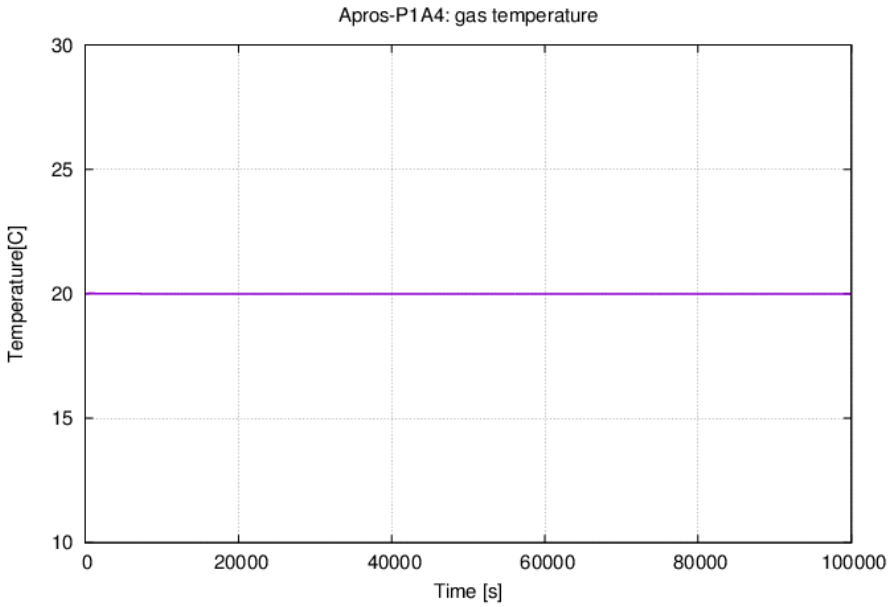

Figure 28. Average gas temperature of the containment vessel (null simulation).

4.2.3.2 Effect of steam injection rate

Three transient cases with different steam injection rates (0.01, 0.02 and 0.03 kg/s) to the containment vessel were simulated. The simulation time was 55.5 hours. The aim of the simulation was to find out suitable steady state (or quasi-state) conditions for the preliminary OpenFOAM simulation. Transient CFD simulation requires much more computing time, therefore, steady state initial boundary conditions were used in the first step. Figure 29 to Figure 31 show that nearly quasi-steady vessel conditions (pressure 2.5 bar, average gas temperature 118 °C, average steam mole fraction 0.57) are reached until the end of simulation with the 0.01 kg/s steam source. If the steam injection rate is higher, even the quasi-steady conditions are not reached during the simulation time of 55.5 hours. Therefore, the following considerations concentrate on the 0.01 kg/s case, but the other simulation cases are also presented in the figures for comparison.

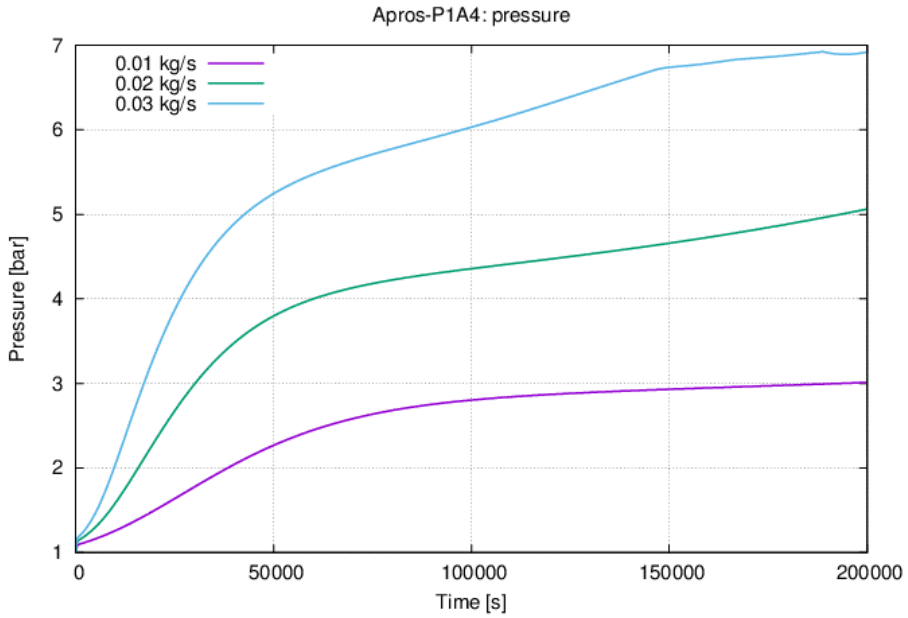

Figure 29. Containment pressure (varied steam injection rate).

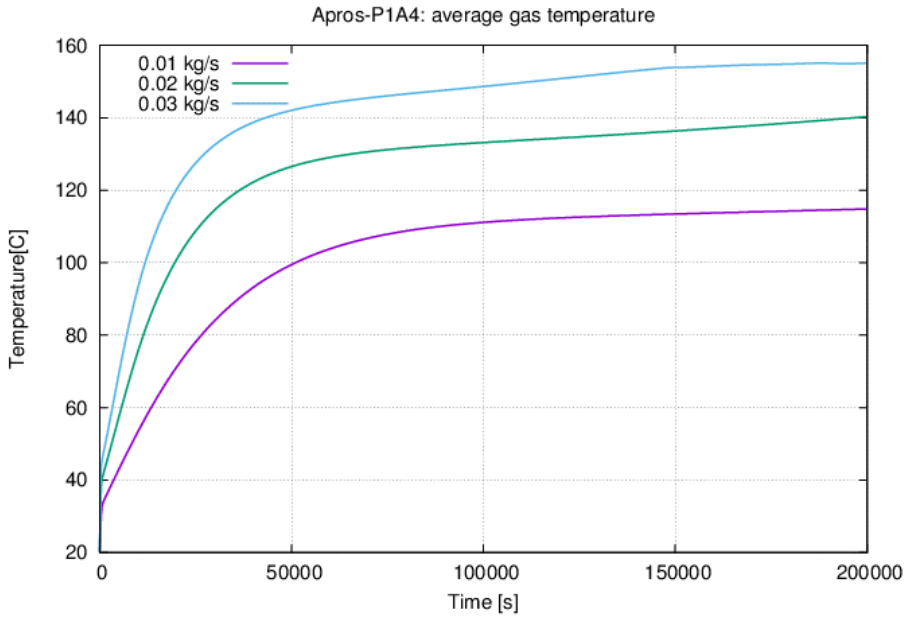

Figure 30. Average containment temperature (varied steam injection rate).

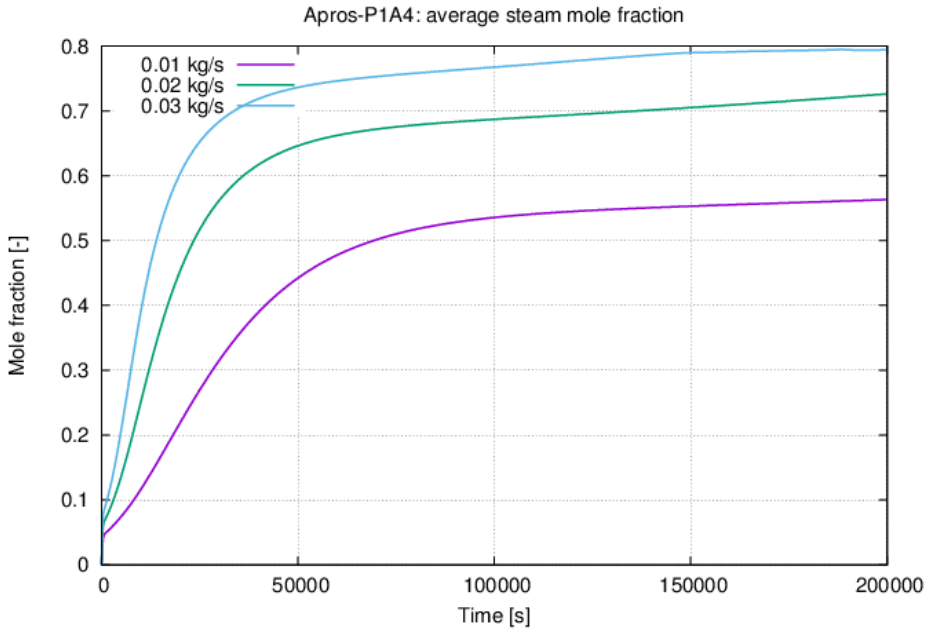

Figure 31. Average steam mole fraction in the containment (varied steam injection rate).

Although the injected steam is slightly superheated, the average relative humidity in the vessel reaches saturation state as expected due to condensation process on the PCCS pipe and vessel walls (Figure 32). This indicates that the combined heat and mass transfer calculation of the Apros model is sound.

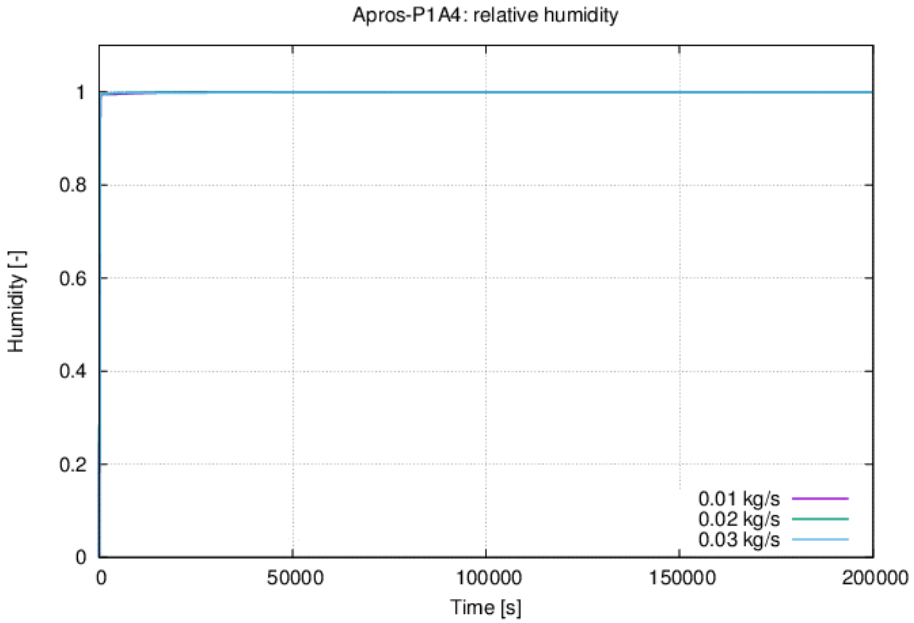

Figure 32. Average humidity in the containment (varied steam injection rate).

The heat flow from the vessel to the PCC pipe and condensation rate on the PCC pipe are shown in Figure 33 and Figure 34.

The quasi-steady heat flow rate is about 20 kW in 0.01 kg/s case and the corresponding condensation rate is about 8 g/s. Strong oscillation in the heat flow and condensation rate starts at about 15 000 s in case of 0.03 kg/s steam injection because a local water boiling occurs in the outlet of the PCC pipe.

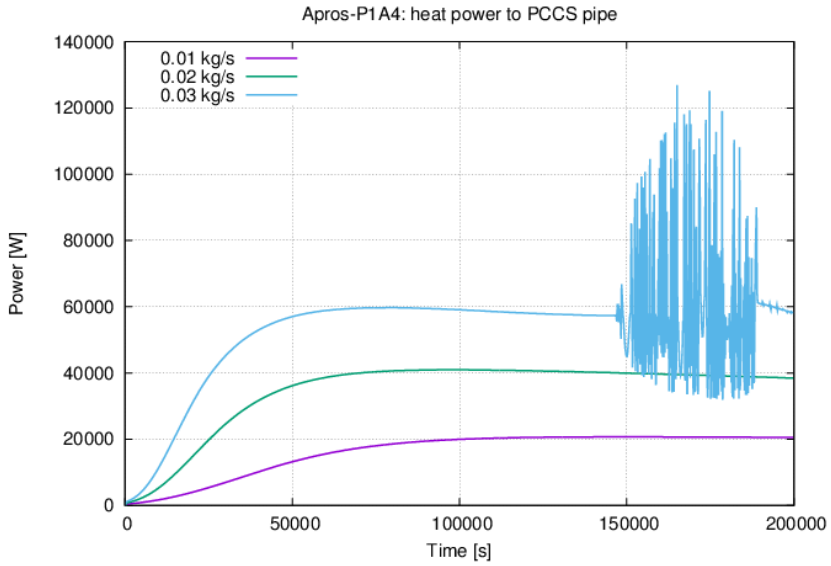

Figure 33. Heat flow from the containment to the PCCS pipe (varied steam injection rate).

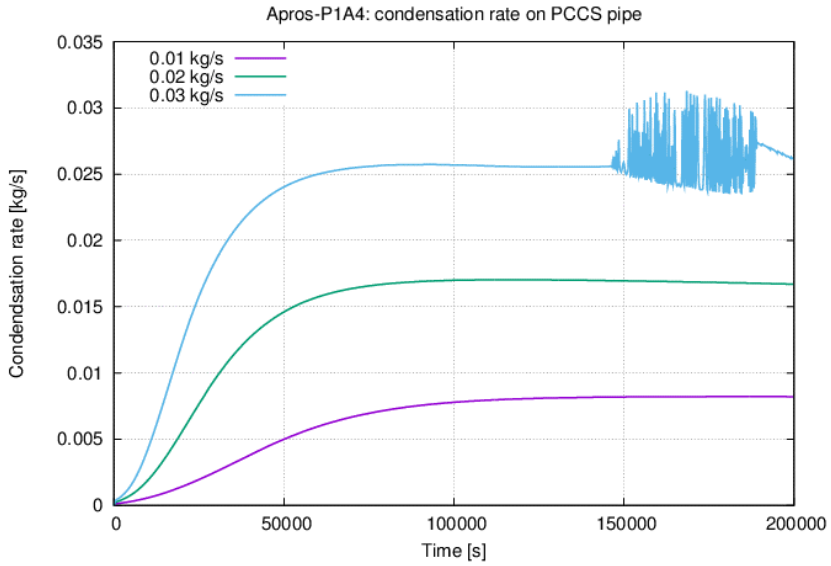

Figure 34. Condensation rate on the PCCS pipe (varied steam injection rate).

The integrated condensation masses on the PCCs pipe and the vessel walls are shown in Figure 35. The condensation on the walls is dominant at an early stage of simulations, but the

condensation on PCC pipe overcomes after a certain moment of time. In the 0.01 kg/s case the condensation on PCC pipe becomes dominant at about 28 h (100 000 s = 27.8 h). With the higher steam mass flow, this takes place earlier. The total condensation masses in the 0.01 kg/s case are 1250 kg on the PCC pipe and 600 kg on the vessel wall (in the end of simulation). Note that the vessel walls were insulated.

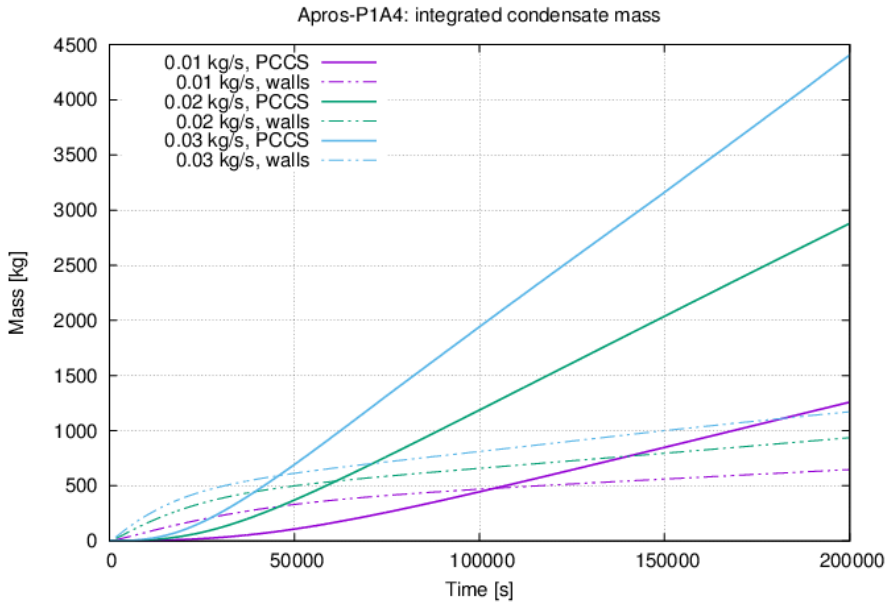

Figure 35. Integrated condensate mass on the PCC pipe and vessel walls (varied steam injection rate).

A quasi-steady water mass flow in the PCC pipe is about 0.25 kg/s in the case of 0.01 kg/s steam injection (Figure 36).

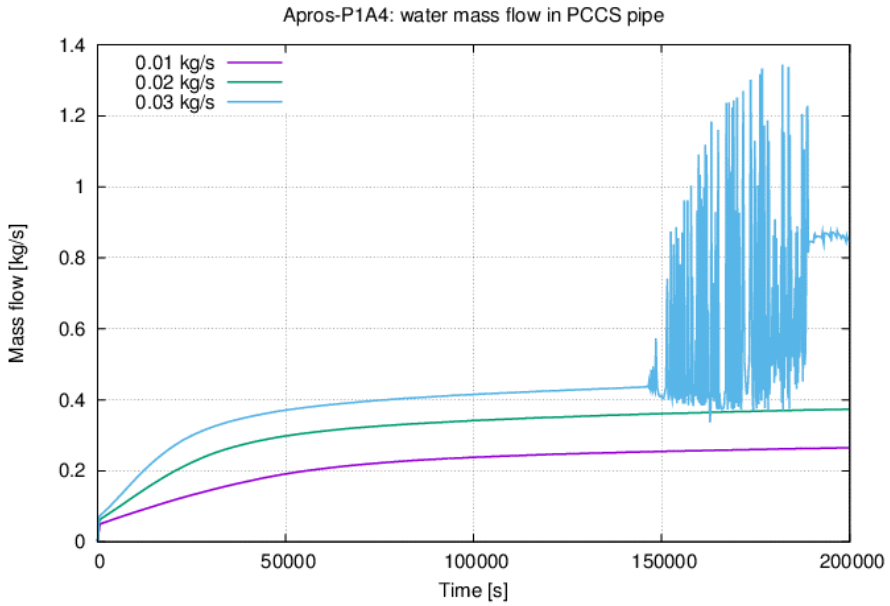

Figure 36. Water mass flow in the PCCS pipe (varied steam injection rate).

The water pool temperature is presented in Figure 37. With the higher steam injection rate to the vessel, also the heat flow from the vessel to the PCCS is higher, and hence, the pool temperature becomes higher.

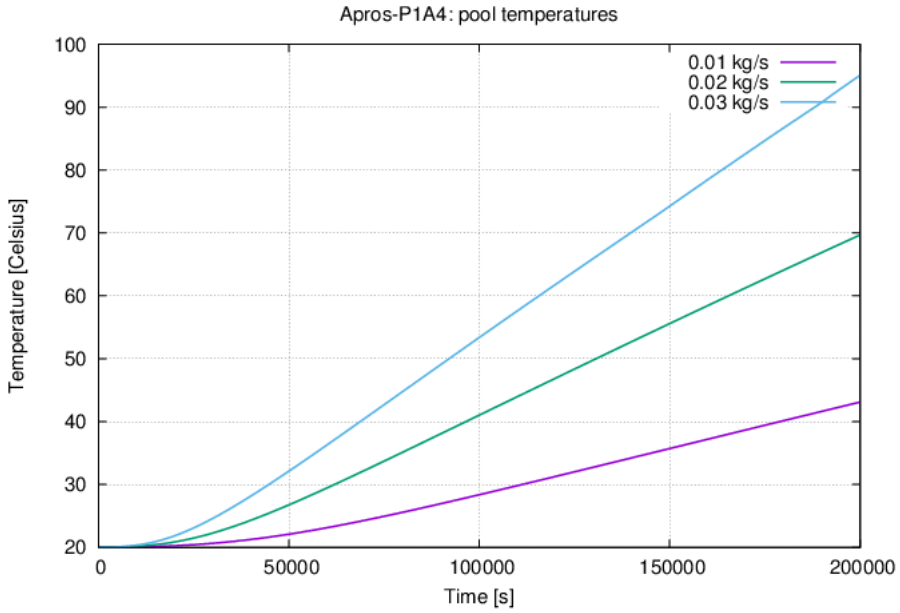

Figure 37. Temperature of the water pool (varied steam injection rate).

Figure 38 presents the steam model fractions at three different vertical elevations in the containment vessel. As seen in the figures, Apros assumes a good mixing of steam and nearly homogeneous conditions. This is probably due to lumped parameter approach and because the steam release location is low in the vessel.

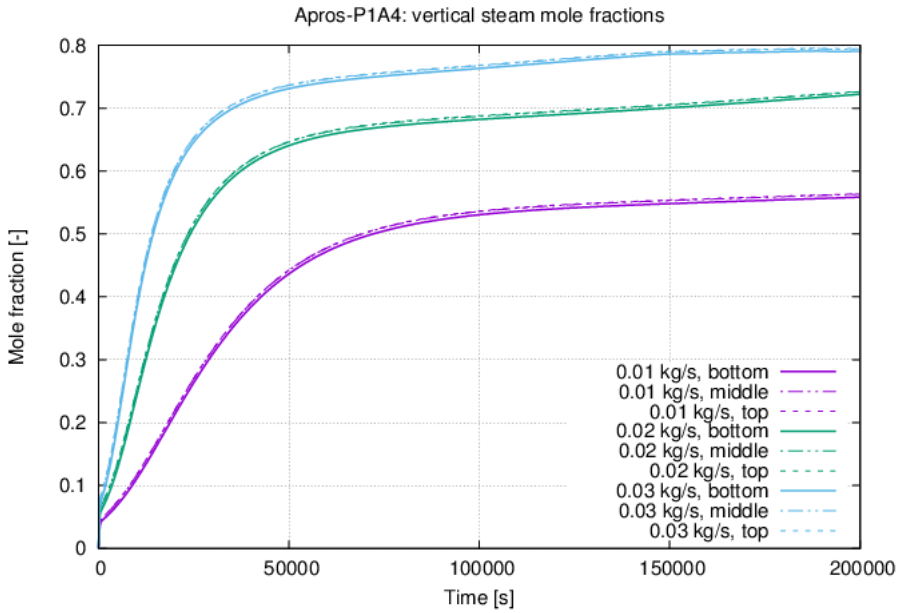

Figure 38. Steam concentrations at three different elevations in the containment vessel (varied steam injection rate).

4.2.3.3 Time step effects

The time step effect was studied assuming a steam injection rate of 0.01 kg/s. The maximum system time steps were varied: 0.005 s, 0.01 s, 0.05 and 0.1 s.

The simulated conditions of the containment vessel are not sensitive to the time steps used as seen in Figure 39 to Figure 41 where the containment pressure, the average gas temperature and the heat power from the containment vessel to the PCC pipe are plotted, respectively. Water natural circulation calculation in PCCS show some sensitivity to given time steps, but only during the first hour of the simulation (Figure 42). This is of minor importance, and hence, a value of 0.05 s was used in the work to guarantee fast-speed simulations.

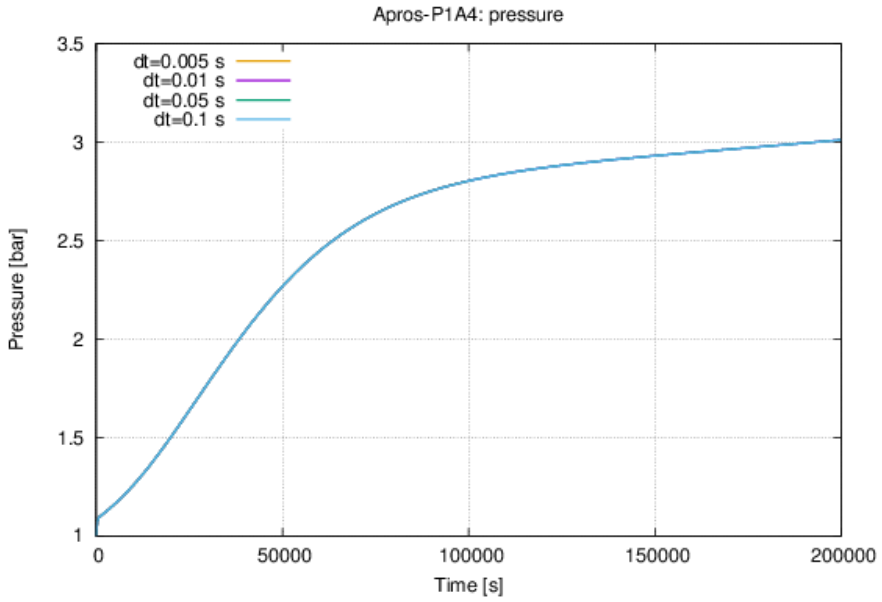

Figure 39. Containment pressure (varied time step).

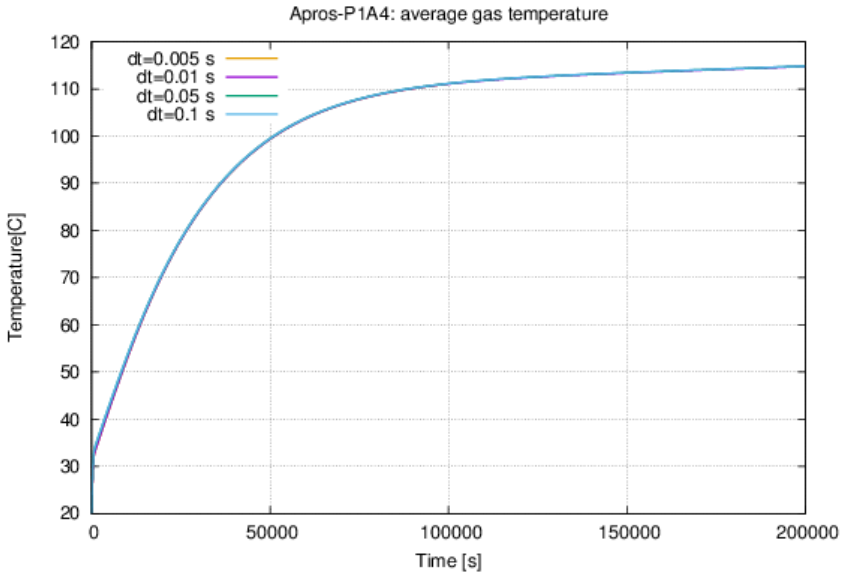

Figure 40. Average containment temperature (varied time step).

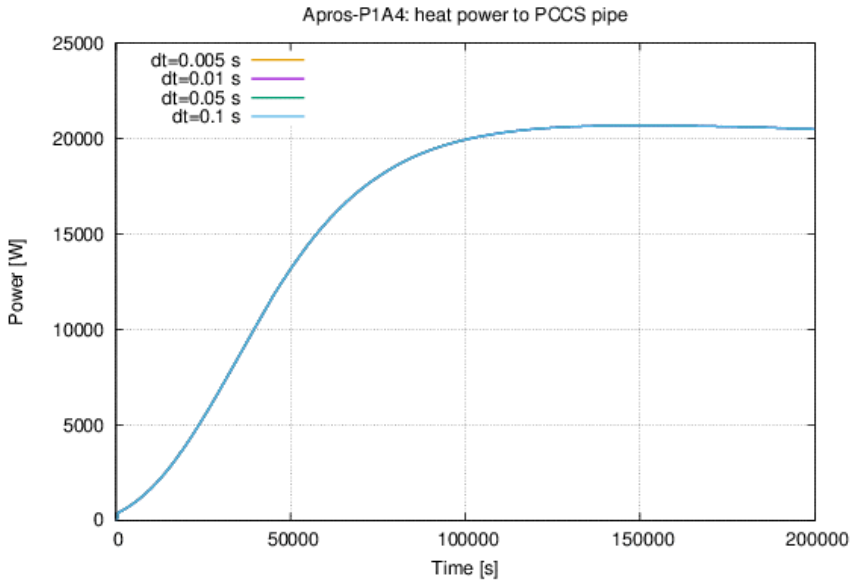

Figure 41. Heat power from the containment vessel to the PCC pipe (varied time step).

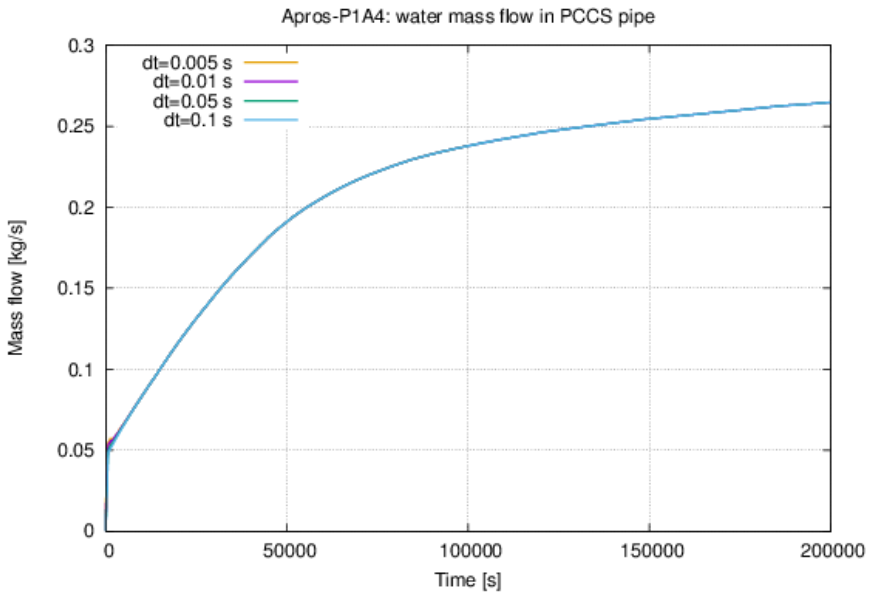

Figure 42. Water mass flow in the PCCS pipe (varied time step).

4.3 CFD modelling with OpenFOAM

4.3.1 Model description

The simplified CAD shown in Figure 43 consisted of the containment vessel, the PCC pipe inside it and the steam injection line. The water pool was excluded. The original pipe diameter of the steam injection was tested. It resulted in large velocities which caused large courant number, reflected on the time step needed to ensure numerical stability to be small. Thus, a larger pipe diameter was used to overcome this limitation. The diameter used was 0.4 m.

Three regions were defined, fluid representing the vessel bulk flow, vessel walls, and steam injection. The coolant flow of the PCC pipe, and the solid representing the walls of the PCC pipe were modelled. The condensation length of the pipe was only modelled based on the assumption that the elbow and the outlet regions are insulated. The mesh used is shown in Figure 44. Number of cells used for this mesh was 428336. The wall of the PCCS pipe was meshed with three thin layers.

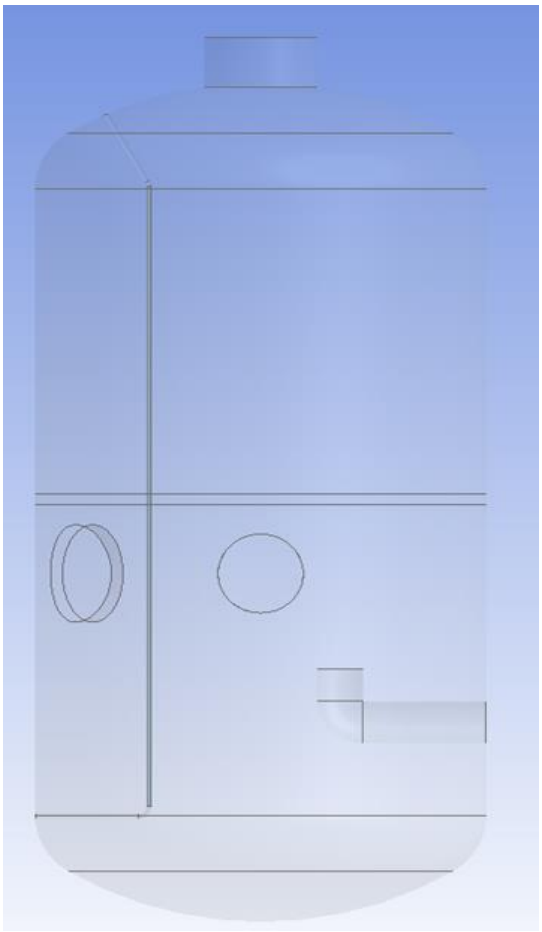

Figure 43. Simplified PANDA CAD

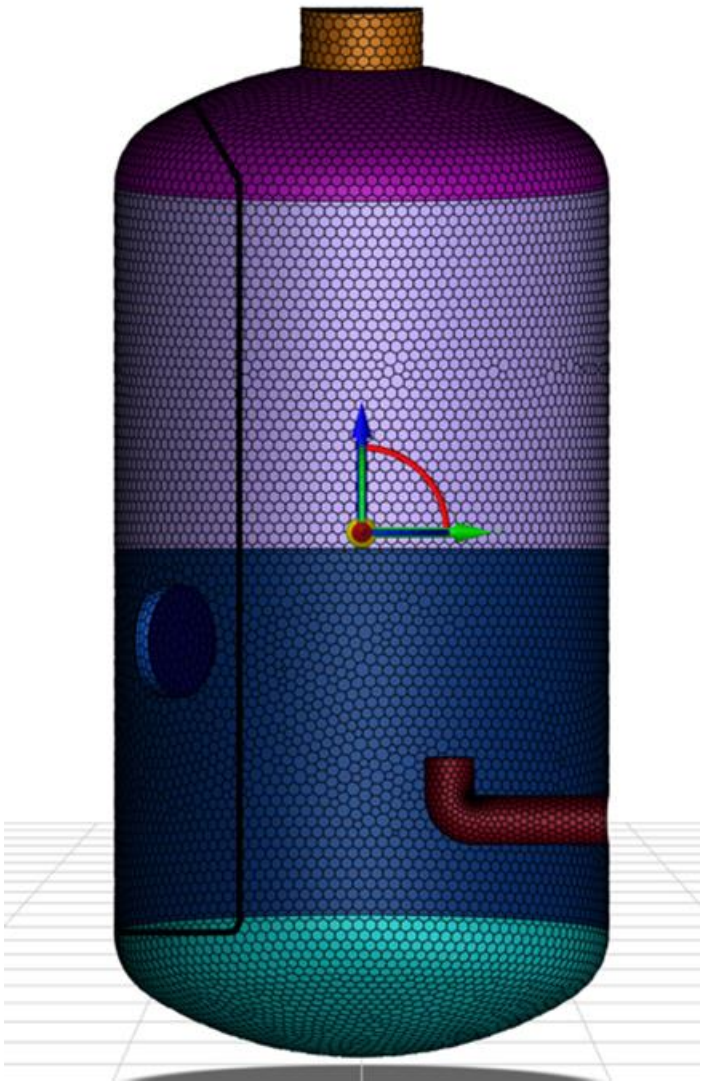

Figure 44. PANDA mesh.

4.3.2 Heat transfer modelling

The different regions were modeled using the conjugate heat transfer method in OpenFOAM. The fluid region was modeled by Eulerian multiphase model for the gas mixture of steam and air. The condensate was modeled as a liquid phase. The simulation was performed used RANS with turbulence model $k-\omega\ SST$.

The condensation model used in this simulation based on diffusion theory was developed by VTT (J.Syrjänen, V.Hovi et al., 2023). The condensation model used assumes that the condensation is dominanted by diffusion. Thus, the condensate film forming on a wall is assumed to be at saturated state at the vapor partial pressure equal to the saturation pressure at the wall temperature. The mass flux of the condensing steam from the wall at distance 0.0 to the boundary layer edge at distance δ is given by the following equation:

$$j_{H_2O} = \frac{M_{H_2O}\ D_{EFF,gas-H_2O}\ \rho}{M\ \delta} \ln\left(\frac{|1.0 - x_{H_2O,\delta}|}{|1.0 - x_{H_2O,0}|}\right) \quad (1)$$

The effective diffusion coefficient is the summation of the laminar term and diffusion due to turbulence. The effective diffusion is defined in equation 2. The turbulent Prandtl Pr_t and Schmidt Sc_t numbers set to 0.85 and 0.7 respectively. The laminar diffusion coefficient for multicomponent gas mixture is given by equation 3.

$$D_{EFF,gas-H_2O} = D_{gas-H_2O} + \frac{Pr_t}{Sc_t}\alpha_t \tag{2}$$

$$D_{gas-H_2O} = \frac{(1.0 - x_{H_2O})}{\frac{x_{N_2}}{D_{N_2-H_2O}} + \frac{x_{O_2}}{D_{O-H_2O}}} \tag{3}$$

The initial conditions used in the OpenFOAM simulation were obtained by running Apros simulation from cold state without injection, then with injection of steam with a rate of 0.01 kg/s. The initial and boundary conditions are summarized in Table 4 where boundary conditions parameters are denoted with "*". Initially the condensed liquid water was collected at the bottom of the tank. However, around 540 seconds the simulation broke due to some numerical issues caused by the evaporation of the condensed liquid. Thus, to continue the simulation the condensed liquid was taken out after 540 seconds.

Table 4. Initial and boundary conditions OpenFOAM.

PCCS pipe				
m_{in} [kg/s]*	T_{in}[℃]*	$T_{w,in}$[℃]	$T_{w,out}$[℃]	$P_{out}[bar]$ *
0.25	20.0	55.0	60.0	1.61
Vessel				
$m_{injection,steam}$ [kg/s]*	T_{in}[℃]	$T_{initial}$ [℃]	$P_{initial}[bar]$	ω_{steam}
0.01	130	112	2.79	0.395

Subscript "in" denotes to PCC pipe inlet, "out" to PCC pipe outlet, "w" to wall.

4.3.3 Simulation results

4.3.2.1 Vessel results

The presented results are taken from the latest time when the simulation reached 1720 seconds. The containment vessel pressure shown in Figure 45 increases in a relatively slow rate. The pressure increase is dominant by the injection of steam and is expected to start stabilizing or reach quasi-steady state as the simulation progresses. Similarly, the average gas mixture temperature in the containment vessel increases (Figure 46). The total condensation rate due to condensation on the vessel inner walls and the PCCS pipe is shown in Figure 47. The total condensation is dominated by the condensation over the PCCS pipe. However, as the simulation approaches steady state the total condensation over the PCC pipe and the vessel walls should approach the injection of steam mass flow rate. The integrated mass of the total and pipe condensation rates is shown in Figure 48.

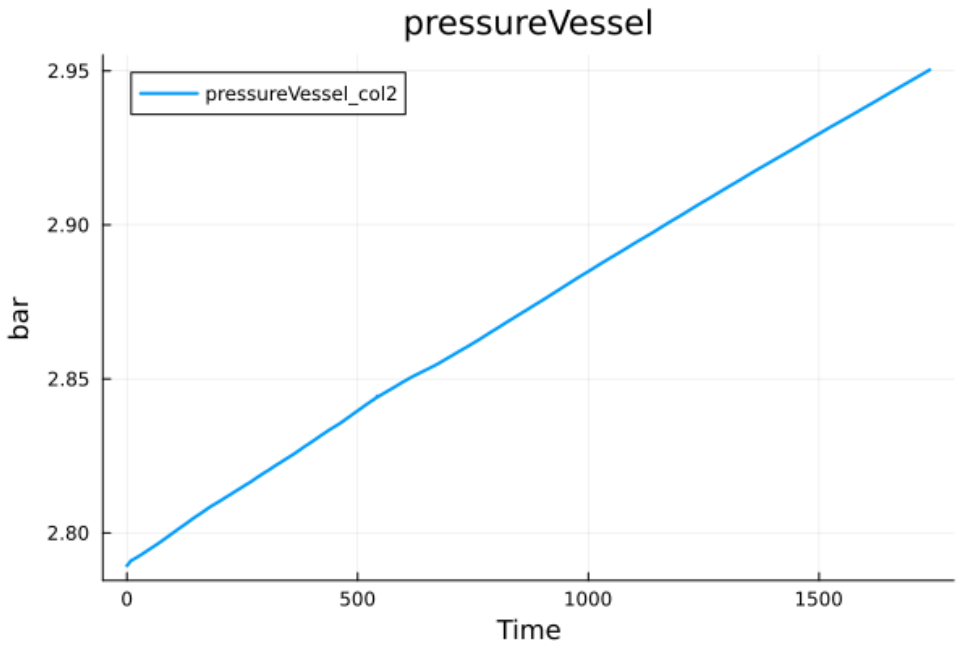

Figure 45. Pressure of the vessel.

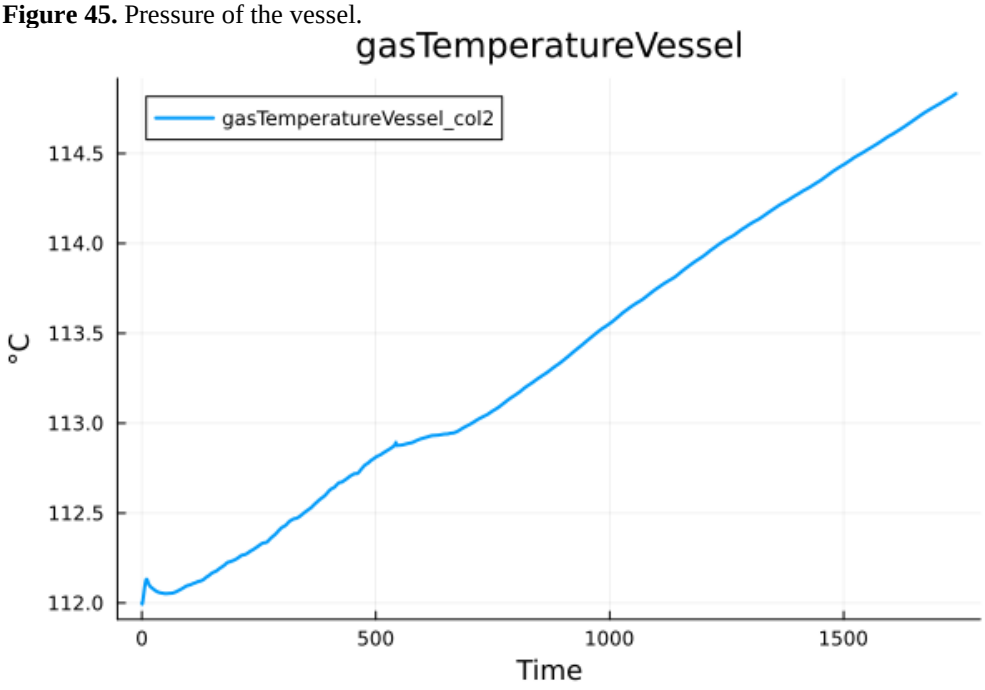

Figure 46. Average gas temperature of the vessel.

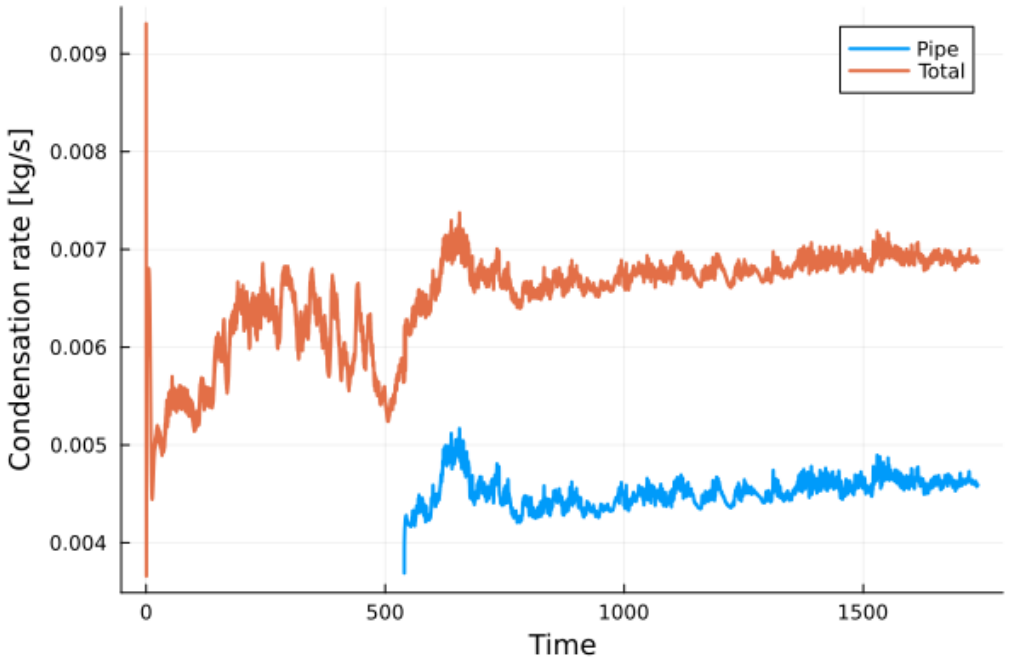

Figure 47. Condensation rate in the vessel.

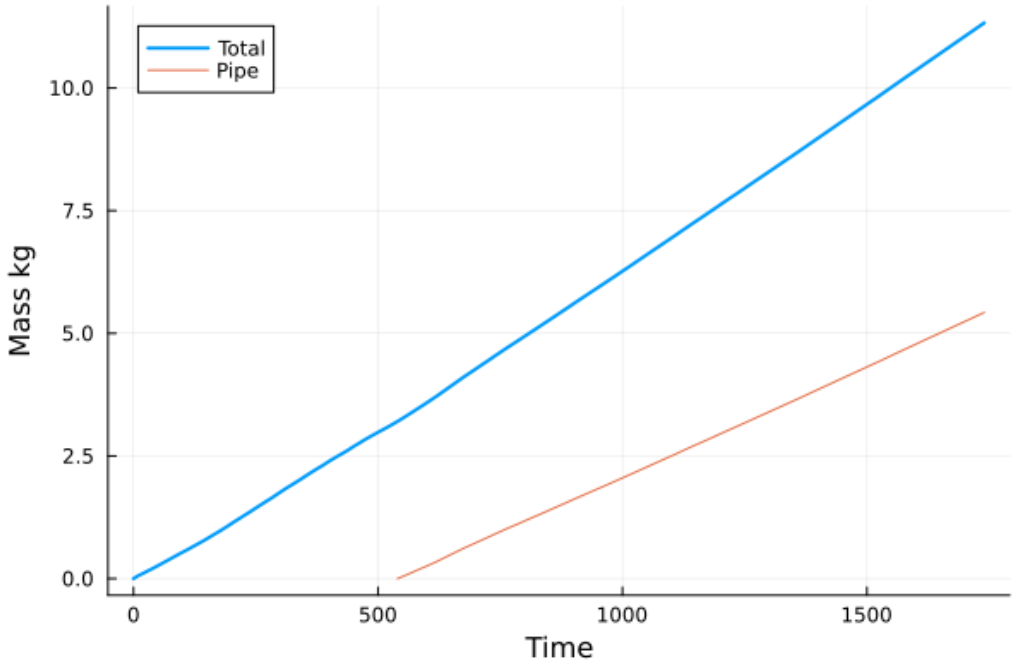

Figure 48. Integrated condensate mass.

The gas mixture velocity streamlines inside the vessel are shown in Figure 49 with the contour of the steam distribution and with the gas mixture temperature distribution in Figure 50. The velocity is qualitatively as expected. The jet dominates the flow as it reaches the top of the vessel resulting in sort of swirling effect which enhances the mixing in the top portion of the vessel. The vessel temperature distribution shows the mixing on the top part. Where the flow shows stratification in the lower part.

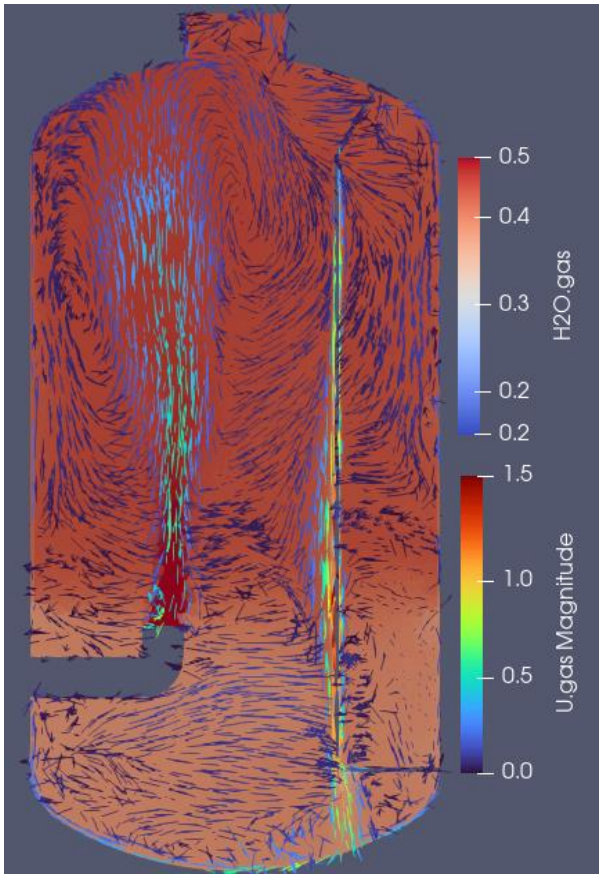

Figure 49. Velocity streamlines with steam distribution

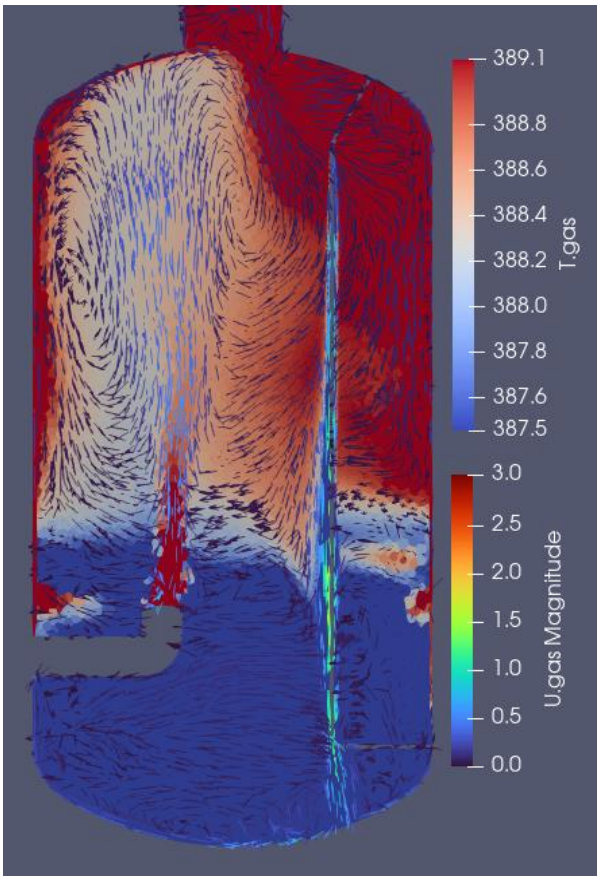

Figure 50. Velocity streamlines with gas mixture temperature distribution

4.3.2.2 Water circuit results

The temperatures along the PCCS pipe and through the pipe walls are shown in Figure 51. The results are qualitatively as expected with the outlet temperature increasing in a slow rate. The temperature through the wall is influenced by the number of cells layers in the wall of the pipe.

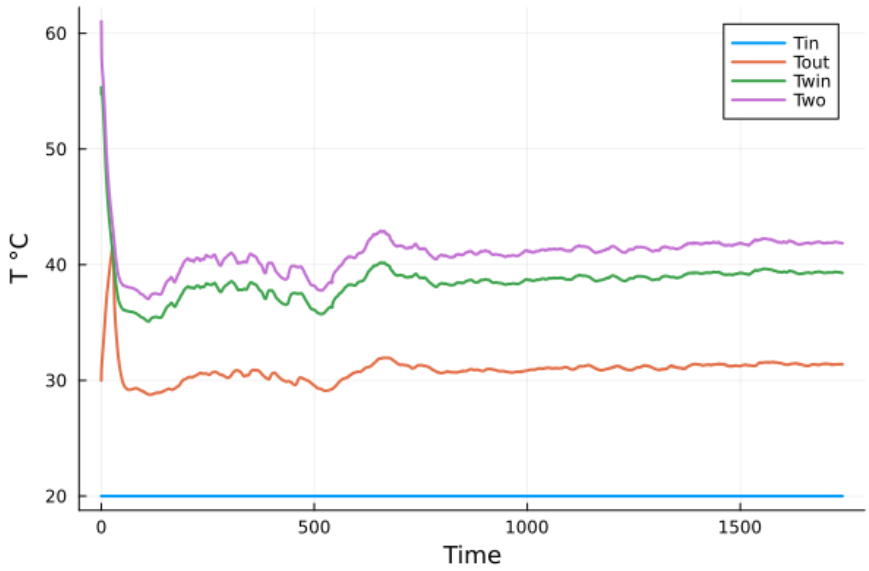

Figure 51. PCCS pipe temperatures.

5. Future work

The Apros heat transfer model (Grimison correlation) for the containment side of the PCC pipe is recommended to be used for tube bank arrangement, and therefore, a suitability of the correlation for a single tube PCCS is questionable. Thus, more suitable heat transfer (and condensation) correlation for a single pipe heat exchanger should be implemented in Apros for future work.

For simplification, a single-node water pool was used in the Apros simulation. Because the pool will be probably stratified in the experiment, a multi-node pool model should be developed for Apros.

The OpenFOAM simulations were performed without well-defined experimental boundary conditions. But the initial and boundary conditions were determined based on Apros. Thus, an improvement regarding the initial and boundary conditions can be carried out when experimental procedure and conditions are defined. Moreover, the injection pipe used was different than what is planned for the facility. This was needed, as explained earlier, to avoid large local velocities that may result in large courant number affected the time step needed to ensure numerical stability to be small. Therefore, an investigation regarding the numerical schemes is recommended. Furthermore, the used mesh is coarse. Thus, a denser mesh can be obtained by refining the regions close to the PCCS pipe and the vessel walls where condensation occur.

6. Conclusions

Apros system code model and the OPenFOAM CFD model were created and the preliminary simulations were conducted for the planned arrangement of the Panda facility PCCS experiment P1A4. The Apros model consisted of the whole system including the containment vessel, the PCC pipe, the PCCS water circulation loop and the water pool. The OpenFOAM model included only the containment vessel, the PCC pipe and the steam injection lines inside the vessel.

Quasi-steady conditions of the whole test apparatus were calculated with Apros varying the steam injection rate. The vessel pressure, gas temperatures, steam mole fractions, water mass flow rate in the PCCS circulation loop and water inlet temperature of the PCC pipe were given as boundary conditions for the CFD simulation. The purpose of the work was to learn and prepare the Apros and CFD model capabilities for future simulation of the Panda test P1A4 to be conducted in the OECD/NEA benchmark exercise.

The Apros results showed that the system model works as expected and the results are qualitatively reasonable. Steam injection rate of 0.01 kg/s seemed to produce quasi-steady conditions during 55 hours simulation.

In conclusion the CFD simulation exceeded 1720 s until finalisation of this report. The preliminary CFD simulation results show qualitative agreement with what it is expected. The total condensation rate increases as more steam condenses. Moreover, slow pressurization trend was shown because of the small injection rate used in the simulations. Velocity contours show the streamlines show the strong mixing in the top part of the vessel with stratification close to the injection.

Some model improvements should be done for the future work. More suitable heat transfer correlation for a single-pipe PCCS should be implemented in Apros. Also a multi-node pool model should be developed.

What comes to the CFD model, an investigation regarding the numerical schemes is recommended. Furthermore, a denser mesh should be developed by refining the regions close to the PCCS pipe and the vessel walls where condensation occurs.

7. References

Hitachi 2023. “BWRX-300 General Description 005N9751 Revision F,” GE Hitachi Nuclear Energy Americas LLC, December 2023.

Incropera, F.P., and DeWitt, D.P. 1990. Fundamentals of Heat and Mass Transfer. Third Edition.

Jeon, S., Hong, S., Park, J. et al. 2013. “Assessment of horizontal in-tube condensation models using MARS code. Part II: Annular flow condensation,” *Nuclear Engineering and Design,* vol. 262, pp. 510-524, 2013.

Jeon, S., Hong, S., Cho, H. et al. 2015. “Prediction of nucleate boiling heat transfer on horizontal U-shaped heat exchanger submerged in a pool of water using MARS code,” *Nuclear Engineering and Design,* vol. 295, pp. 317-337, 2015.

Kapulla, R., Paranjape, S., Fehlmann, M. et al. 2022. “The effects of activated cooler power on the transient pressure decay and helium mixing in the PANDA facility,” *Nuclear Engineering and Technology,* vol. 54, pp. 2311-2320, 2022.

Lee, J., Park, Y., Jeon, S. et al. 2024. “Assessment of MARS-KS prediction capability for natural circulation flow in passive heat removal system,” *Nuclear Engineering and Technology,* PREPRINT.

Lübbesmeyer, D., Aksan, S.N. 2023. “ISP42 (PANDA Tests) Open Phase Comparison Report NEA/CSNI/R(2003)7,” OECD/NEA, May 2003.

Mascari, F., Bersano, A., Alcaro, F. et al.. 2023. “OECD/NEA/CSNI/WGAMA PERSEO benchmark: Main outcomes and conclusions,” *Nuclear Engineering and Design,* vol. 405, p. 112220.

Narcisi, V., Melchiorri, L., Giannetti, F. 2021.“Improvements of RELAP5/Mod3.3 heat transfer capabilities for simulation of in-pool passive power removal systems,” *Annals of Nuclear Energy,* vol. 160, p. 108436, 2021.

Paladino, D., Kapulla, R., Paranjape, S. et al. 2022.“PANDA experiments within the OECD/NEA HYMERES-2 project on containment hydrogen distribution, thermal radiation and suppression pool phenomena,” *Nuclear Engineering and Design,* vol. 392, p. 111777, 2022.

Paladino, D., Kapulla, R., Paranjape, S. et al., 2023. “PANDA experimental database and further needs for containment analyses,” *Nuclear Engineering and Design,* vol. 404, p. 112173, 2023.

Pomogaev, A. 2022. “BWRX-300 isolation condenser system analysis, Master's Thesis,” Lappeenratna-Lahti University of Technology LUT, 2022.

Paranjape, S., Kapulla, R., Kudinov, P. et al. 2024. “Experimental results of thermocline evolution in a water pool under combined effect of steam venting and water injection,” *Nuclear Engineering and Design*, vol. 419, p. 112914, 2024.

Rivera, Y., Paladino, D., Kapulla, R., Chae, M.S., Ghendour, N., Hug, V., Suter, S. 2024. P1A4 series update: towards the definition of PANDA tests. 6th Meeting of the OECD/NEA PANDA project. 03 – 05 June, 2024. Villigen PSI, Switzerland.

Silde, A., Ylijoki, J., Ahtinen, E. 2019. Containment model library of the Apros process simulation software: an overview of development and validation work. Progress in Nuclear Energy 116 (2019) 28 – 45.

Syrjänen, J., Hovi, V. et al., 2023. Validation of a surface condensation model for PWR containment analysis, Espoo: VTT.

Szogradi, M and Alblouwy, F. 2025. European SMR station blackout thermal-hydraulic analysis with the Apros system code. To be published in Elsevier.

Bibliographic Data Sheet **NKS-493**

Title	CFD and system code modelling of passive safety system performance
Author(s)	Ari Silde, Afeef Murad, Marton Szogradi
Affiliation(s)	VTT Technical Research Centre of Finland Ltd.
ISBN	978-87-7893-590-8
Date	January 2025
Project	NKS-R / PAS-SMR
No. of pages	50
No. of tables	4
No. of illustrations	51
No. of references	16

Abstract
max. 2000 characters

Apros system code model and the OPenFOAM CFD model were created and the preliminary simulations were conducted for the planned arrangement of the Panda facility PCCS experiment P1A4. The Apros model consisted of the whole system including the containment vessel, the PCC pipe, the PCCS water circulation loop and the water pool. The OpenFOAM model included only the containment vessel, the PCC pipe and the steam injection lines inside the vessel.

Quasi-steady conditions of the whole test apparatus were calculated with Apros varying the steam injection rate. The vessel pressure, gas temperatures, steam mole fractions, water mass flow rate in the PCCS circulation loop and water inlet temperature of the PCC pipe were given as boundary conditions for the CFD simulation. The purpose of the work was to learn and prepare the Apros and CFD model capabilities for future simulation of the Panda test P1A4 to be conducted in the OECD/NEA benchmark exercise.

The Apros results showed that the system model works as expected and the results are qualitatively reasonable. Steam injection rate of 0.01 kg/s seemed to produce quasi-steady conditions during 55 hours simulation.

The CFD simulation exceeded 1720 s until finalisation of this report. The preliminary CFD simulation results were promising.

Some model improvements should be done for the future work. More suitable heat transfer correlation for a single-pipe PCCS should be implemented in Apros. Also a multi-node pool model should be developed.

What comes to the CFD model, an investigation regarding the numerical schemes is recommended. Furthermore, a denser mesh should be developed by refining the regions close to the PCCS pipe and the vessel walls where condensation occurs.

Key words SMR, BWRX-300, passive safety system, modelling, Apros, OpenFOAM